Seasonal and Geologic Controls on Submarine Groundwater Discharge-Derived Nutrient Fluxes to Two Coastal Embayments

M. Taylor[1], J. Tamborski[1], A. Alorda-Kleinglass[1], N. Maynard[1]

[1]Department of Ocean and Earth Sciences, Old Dominion University, Norfolk, VA, USA.

Corresponding author: Moira Taylor (mtayl059@odu.edu)

Key Points:

- Season and sediment type govern submarine groundwater and porewater flow, shaping nutrient speciation and flux.
- Pairing groundwater nutrient loads with coastal subsurface production or consumption rates allows for a more comprehensive nutrient budget.
- Longer, deeper coastal groundwater flow paths yield among the highest loads of ammonium, phosphate, and silicate.

Abstract

Submarine groundwater discharge and porewater exchange are critical but often overlooked sources of nutrients to coastal systems. This study investigates how sediment permeability and seasonality influence the magnitude and biogeochemistry of nutrient fluxes from submarine groundwater discharge and porewater exchange. Reaction rates in the subterranean estuary were used to identify the transformations and drivers of nutrient loading to two geologically distinct embayments on the U.S. east coast: the highly permeable Peconic Bay estuary (NY), and the surficially fine-grained coastal embayments of the southern Delmarva Peninsula (VA). We then applied radium isotope mass balances to distinguish total submarine groundwater discharge and porewater exchange contributions to identify the dominant nutrient pathways. Seasonal comparisons of Peconic Bay revealed that increased surficial aquifer recharge in winter lead to a seaward shift of the freshwater-saltwater interface and elevated submarine groundwater discharge, whereas porewater exchange remained seasonally stable. In contrast, the Eastern Shore showed higher rates of submarine groundwater discharge and nutrient production, despite the lower permeability at the sediment surface, highlighting the influence of deeper aquifer permeability. Nutrient fluxes were tightly coupled to both the water flux and nutrient transformations within the subterranean estuary, largely governed by oxygen availability, with submarine groundwater discharge dominating nutrient delivery in winter and fine-grained sediments enhancing ammonium, phosphate, and silicate production. These findings highlight the importance of hydrogeologic setting and seasonal forcing in controlling the role of coastal aquifers in nutrient cycling in shallow coastal embayments.

Plain Language Summary

Groundwater flowing into the ocean and water moving through coastal sediments are important sources of nutrients, but they are often overlooked. We studied how seasonal changes and sediment type affect these nutrient flows in two very different coastal systems on the U.S. East Coast. In sandy sediments of Peconic Bay, New York, we found that reduced municipal pumping combined with increased precipitation during the winter increased groundwater discharge into the ocean, while water moving through surficial coastal sediments stayed steady year-round. In Virginia's Eastern Shore, where surface sediments were less permeable, deeper aquifers supplied more groundwater and nutrients. Nutrient delivery depended on both the amount of water moving through sediments and chemical reactions underground, which were influenced by

oxygen levels. Groundwater discharge into the ocean peaked in winter compared to summer, reflecting strong seasonal controls, while sediment type shaped nutrient cycling, with fine-grained sediments promoting the production of nutrients like ammonium, phosphate, and silicate. These findings show how geology and seasons shape the way coastal aquifers contribute to nutrient cycling.

1. Introduction

Nutrient excess in coastal systems can lead to eutrophication, resulting in poor water quality, fish kills, and declines in recreation and tourism (Bortman & Niedowski, 1998). Shallow, coastal embayments are particularly vulnerable to eutrophication due to their shallow depths and restricted circulation (Giordano et al., 2011). Anthropogenic nutrient inputs into coastal systems can affect coastal primary production (Lecher et al., 2015) and disrupt marine ecosystems (Lecher et al., 2018). While nutrient loading to coastal systems is often attributed to fertilizer use, sewage and landfill contamination (Lecher et al., 2018) transported by surface water runoff and rivers (Wilson et al., 2024c), groundwater can also be a significant pathway for nutrients (Rodellas et al., 2018). Often, nutrient fluxes via submarine groundwater discharge (SGD) can rival or exceed those from rivers (Slomp & Van Cappellen, 2004; Wilson et al. 2023; Wilson et al. 2024c).

SGD plays a key role in coastal nutrient budgets by transporting water and solutes from land to coastal oceans (Moore, 2010). Despite its importance, SGD has often been neglected as a contributing source of eutrophication, especially for nitrogen (Scavia & Bricker, 2006; Brandes et al., 2007; Santos et al., 2008). SGD varies across spatial (meters to kilometers) and temporal (hours to days) scales (Garcia-Orellana et al., 2021). Here, SGD is divided into two components: fresh submarine groundwater discharge (FSGD) and marine submarine groundwater discharge (MSGD), the sum of which is total submarine groundwater discharge (TSGD). FSGD consists of meteoric terrestrial water driven primarily by hydraulic gradients (Xu et al., 2024; Santos et al., 2010). MSGD results from recirculated seawater driven by changes in sea level, seasonal migration of the freshwater-saltwater interface, tidal pumping, and density-dispersion along the freshwater-saltwater interface with scale lengths greater than meters (Santos et al., 2012; Xu et al., 2024; Taniguchi et al., 2019). SGD differs from porewater exchange (PEX), which occurs on smaller spatial (centimeters) and temporal ($\leq$ minutes) scales. PEX is primarily driven by bioirrigation, wave pumping, and ripple migration (Santos et al., 2012). Distinguishing SGD

from PEX is important as their differing residence times affect interactions between water and sediments, leading to distinct biogeochemical characteristics (Taniguchi et al., 2019).

The mixing of fresh and saline waters in the coastal aquifer forms the subterranean estuary (STE), a major biogeochemical reaction zone (Moore, 1999). The STE can consist of strong gradients of salinity, pH, redox conditions, and nutrient concentrations over potentially small spatial scales, which can influence nutrient transformations and fluxes supplied via SGD or PEX to the coastal ocean (Santos et al., 2008). Within this zone, strong geochemical gradients can drive a range of reactions. Processes of nitrification, denitrification, and dissimilatory nitrate reduction to ammonium are biologically-mediated (Ruiz-González et al., 2021), while geochemically-mediated processes include the sorption and desorption of phosphate, and the weathering (production) or secondary phase formation (consumption) of silica (Santos et al., 2021; Slomp & Van Cappellen, 2004). These reactions can attenuate nutrient fluxes via organic matter decomposition and nutrient regeneration, sorption, or precipitation. The balance of these reactions can control whether the STE is a source or sink of nutrients to the coastal ocean. Understanding the STE and its driving role in nutrient cycling is essential for assessing the potential contribution of SGD to coastal eutrophication.

Radium and radon isotopes are widely used as SGD and PEX tracers, and for estimating residence times in coastal systems, due to their unique radioactive and chemical properties (Moore, 2010). Radium concentrations in brackish groundwaters can be orders of magnitude higher than in seawater (Garcia-Orellana et al., 2021; Swarzenski, 2007; Charette et al., 2008). The radium quartet is useful for tracing SGD processes across various spatial and temporal scales of land-sea processes due to their differing half-lives: ^{223}Ra ($t_{1/2}$ = 11.4 d), ^{224}Ra ($t_{1/2}$ = 3.6 d), ^{226}Ra ($t_{1/2}$ = 1600 y), ^{228}Ra ($t_{1/2}$ = 5.75 y) (Moore, 2010). Radon (^{222}Rn) complements the radium quartet as a tracer because of its short half-life ($t_{1/2}$ = 3.8 d) and non-dependency on salinity, making it especially useful for assessing recent groundwater discharge (Burnett & Dulaiova, 2003) and short residence times (Tamborski et al., 2017a) in coastal and continental groundwaters. Together, radon and the radium isotope quartet provide a suite of tracers that can constrain residence times across a wide range of temporal scales, from days to years.

In groundwater-dominated systems, nitrogen loading model (NLM) frameworks often reduce upland nitrogen inputs by attenuation factors (Kelly et al., 2021; Valiela et al., 1997), and those factors can be among the most sensitive terms within the model (Kelly et al., 2021). Along

the subsurface flow paths, however, nitrogen is reworked as it can be converted to other forms, removed, or generated, so traditional NLM-based attenuation factors may underestimate nitrogen loads to embayments. NLMs omit production transformations that may occur within the STE, a potentially critical component of coastal nutrient budgets. While many coastal studies have used radionuclide mass balance approaches to quantify nutrient fluxes (Rocha et al., 2015; Tamborski et al., 2017b; Rodellas et al., 2018), and others have identified reactions within the STE to track nutrient transformations (Santos et al., 2008; Wilson et al., 2024a), these approaches are often applied separately rather than in combination. By integrating nutrient reaction rates with mass balance flux estimates, our study provides a more complete picture of coastal nutrient cycling. This framework separates FSGD and MSGD from PEX, quantifies their water and nutrient fluxes, and determines the rates of production and consumption that shape them. We adjust FSGD nutrient fluxes for transformations that occur as it flows through the STE. By linking these pathways with reaction rates, we show how seasonality and permeability are suggested to drive these biogeochemical conditions and nutrient transport to coastal embayments. Applied to two sites, this approach explains site-specific differences in nutrient delivery and provides a more complete view of nutrient loading to coastal waters. This work advances our understanding of the physical and biogeochemical processes that can drive nutrient export from coastal aquifers.

1.1. Site Descriptions

We examine two geologically distinct but similarly sized embayments in the Northern Atlantic Coastal Plain (Figure 1): the permeable Peconic Bay Estuary of Long Island, New York (hereafter “Peconic Bay”) and the surficially fine-grained coastal bays of the Southern Delmarva Peninsula, Virginia (hereafter “Eastern Shore”). These contrasting settings allow us to assess the role of sediment structure in regulating SGD flow paths and to evaluate seasonal variation in nutrient cycling. Particular attention is given to the seaward migration of the freshwater-saltwater interface during winter recharge and its connection to changes in SGD and nutrient transport.

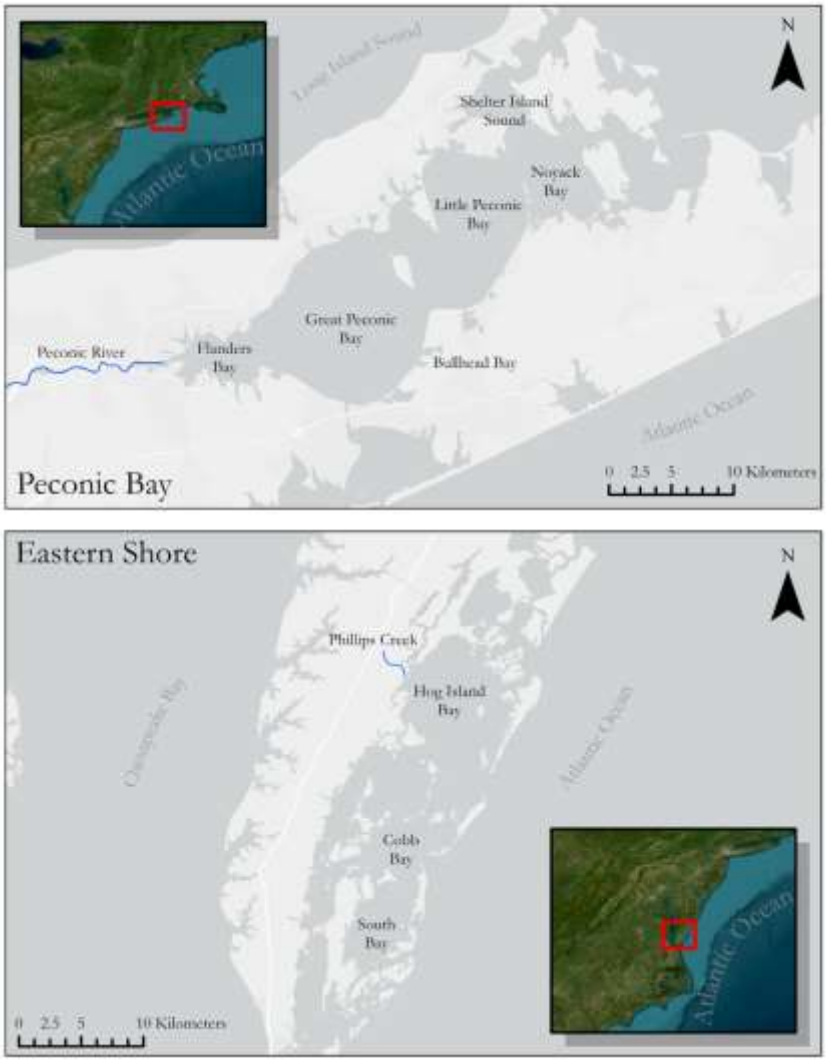

Figure 1. Map of study areas along the U.S. East Coast showing Peconic Bay, Long Island, New York ("Peconic Bay") (top) and the Southern Delmarva Peninsula, Virginia ("Eastern Shore") (bottom).

1.1.1. Peconic Bay

The Peconic Bay (164 km^2) is a series of interconnected bays situated between the North and South Forks of Long Island (New York), extending from Flanders Bay in the west, followed by Great Peconic Bay, Little Peconic Bay, Noyack Bay, and Shelter Island Sound to the east (Figure 1). The estuary receives freshwater input primarily from the Peconic River; regional annual precipitation is up to 116 cm (Schubert, 1998). It exchanges water with Long Island Sound and the Atlantic Ocean through two tidal channels *via* Shelter Island Sound (Hardy, 1976;

Bortman & Niedowski, 1998). The estuary experiences semidiurnal tides (0.7 – 0.8 m range) and depths ranging from 4.3 to 29 m, with circulation driven by tides and wind (Bortman & Niedowski, 1998).

The hydrogeology consists of a surficial unconfined Pleistocene glacial aquifer composed of sandy, highly permeable glacial outwash deposits (Walter et al., 2020) overlying the confined Magothy and Lloyd aquifers, which are composed of sands, gravels, and silty clays, underlain by crystalline bedrock (Fetter, 1976; McClymonds & Franke, 1972). Land use within the watershed includes a mix of agriculture, residential and suburban development (with extensive septic systems and cesspools; Lloyd, 2014), industrial areas, and forested lands (Eckhardt et al., 1986). Peconic Bay has a history of eutrophication, including recurring harmful algae blooms (e.g., Brown Tide), which have contributed to declines in fisheries, eelgrass beds, and shellfish populations (Schubert, 1998). Nitrogen Total Maximum Daily Load (TMDL) regulations have been implemented to curb nutrient inputs and improve water quality (Peconic Estuary Program, 2020).

1.1.2. Eastern Shore

The Eastern Shore (252 km^2) consists of a series of coastal embayments, including South Bay, Cobb Bay, and Hog Island Bay, bound by the southern Delmarva Peninsula to the west and a chain of barrier islands to the east, which separate these tidal lagoons from the Atlantic Ocean (Figure 1). Freshwater enters the system through the discharge of several creeks (Stanhope et al., 2009); average annual precipitation is approximately 30.5 cm (Dillow & Greene, 1999). Deep tidal inlets segment the barrier islands, providing exchange with the Atlantic. It experiences a semidiurnal tidal range of approximately 1.2 m, with water depths generally less than 2 m, though tidal channels can exceed 10 m (Oertel et al.,1989). The elongated shape of the bays allows for significant fetch, promoting bottom resuspension.

On the peninsula lies the surficial Columbia aquifer, overlying the upper, middle, and lower Yorktown-Eastover aquifers (Stanhope et al., 2009). The Columbia consists of silty to gravelly sands with interbedded clay and silt, while the deeper Yorktown-Eastover units, deposited from the late Miocene to Pleistocene, contains transgressive-regressive marine facies of sands and shell material (Richardson, 1994; McFarland & Beach, 2019). Lagoonal sediments are characterized by alternating fine-grained muds and storm-delivered sands reflecting dynamic depositional processes (Oertel et al., 1989). The surrounding landscape is predominantly rural

and uninhabited, dominated by forest, agriculture, and conservation land, with limited industry aside from two poultry processing plants in the north (McFarland & Beach, 2019). This region experiences periodic macroalgal blooms, and their decomposition can lead to localized summer anoxia in Hog Island Bay (McGlarthery et al., 2001; Stanhope et al., 2009). Organic matter and nutrients have been identified to be highest closest to the peninsula, decreasing moving offshore (Tyler, 2002), and it is suggested that most of the dissolved nitrogen in this area comes from groundwater seepage (Reay et al., 1992; Tyler, 2002) and atmospheric deposition (Paerl et al., 1990; Tyler, 2002).

2. Materials and Methods

2.1. Field Methods

Week-long field campaigns occurred in June 2023 for the Eastern Shore, and in August 2023 and December 2023 for Peconic Bay. Groundwater samples were collected across a range of spatial settings, including the intertidal and subtidal zone, using a combination of shoreline access, wading, and shallow boat-based sampling. In August 2023, the Peconic Bay subtidal groundwaters were sampled directly from shore (n = 11) and from shallow boat work (n = 8), between 0 and 100 m offshore. In December 2023, the Peconic Bay intertidal and subtidal groundwater samples were collected directly from shore and by wading up to 10 meters offshore (n = 16). All Eastern Shore groundwater samples were collected by boat, up to 9 km from the mainland, reflecting the exceptionally flat bathymetry of the Eastern Shore's back-barrier lagoon system (n = 12). All groundwater samples were collected using a peristaltic pump connected to a push-point or drive-point piezometer (Charette & Allen, 2006). Samples were taken from various depths, ranging from just below the sediment surface to 185 cm, after purging at least three volume equivalents.

In Peconic Bay, 34 surface water stations were sampled in August and 25 in December. Two river samples were collected each season in the Peconic River, one freshwater sample at the USGS gauging station upstream (USGS #01304500), where discharge data of the month prior to sampling was obtained, as well as a brackish sample at the mouth of the Peconic River. Twenty-one surface water stations were sampled for the Eastern Shore. To represent creek inputs into the Eastern Shore embayments, geochemical measurements were measured at high tide and at low tide at the mouth of Phillips Creek, which drains into the embayment. These creek samples were

assumed to be representative of the six additional creeks discharging into the Eastern Shore coastal embayments during this time.

Groundwater samples (>2 L) were collected for radium analysis, and MnO_2-coated acrylic fibers were added to the collection bottles to adsorb dissolved radium. The water sample and fibers were frequently stirred for 15 minutes to ensure sufficient contact between the fibers and the water. Reducing groundwaters (< 0 mV) were oxidized with sodium hypochlorite to avoid reduction of the MnO_2 fibers. Groundwater radon was collected, bubble-free, in 250 mL glass bottles with no headspace. Surface water and river samples were pumped from ~0.5 m depth using a submersible pump into a cubitainer for radium (22.5 – 45 L). The cubitainers were gravity-drained at <1 L min^{-1} through cartridges with MnO_2 fibers. Surface water and river samples for ^{222}Rn were collected, also using a submersible pump, into triple rinsed 8 L HDPE jerricans immediately sealed with a with a 3-way manifold lid for ^{222}Rn analysis, following the method outlined by Stringer and Burnett (2004). For nutrients, 50 – 100 mL was filtered (0.45 µm cartridge filter in line with 0.2 µm), collected in Falcon tubes and immediately frozen. All water quality parameters were continuously monitored (pH, salinity, temperature, oxidation-reduction potential, dissolved oxygen) using a calibrated In Situ Aqua TROLL 600 Multiparameter Sonde and documented once the parameters stabilized.

2.2. Analytical Methods

The MnO_2 fibers were triple-rinsed with radium-free deionized water to remove salts and particles, then dried following the procedure in Moore (2008). Short-lived isotopes (^{223}Ra and ^{224}Ra) were analyzed on a radium delayed coincidence counter (RaDeCC) 1-2 days after sample collection following Moore and Arnold (1996), with modifications by Diego-Feliu et al. (2020). Efficiencies were determined from ^{232}Th standards for ^{224}Ra, and following Moore and Cai (2013) for ^{223}Ra. Excess ^{224}Ra was determined by recounting the samples one month after collection to quantify ^{228}Th, which was then used to calculate the amount of unsupported ^{224}Ra. Uncertainty for ^{223}Ra and ^{224}Ra were calculated by error propagation, incorporating detector efficiency, decay correction, and chance coincidence correction (Garcia-Solsona et al., 2008; Diego-Feliu et al., 2020); all ^{224}Ra reported is as excess ^{224}Ra. Long-lived ^{228}Ra was quantified following Moore (2008) by recounting the samples >6 months after collection for ^{228}Th ingrowth via RaDeCC.

Subtidal groundwater samples of ^{222}Rn were analyzed using a closed-loop radon-in-air monitor (RAD7/RAD8; Durridge Co.), where radon was equilibrated between the water sample and air loop and its activity was calculated based on the partitioning factor for water temperature and salinity (Schubert et al., 2012). Analyses were performed the same day, with decay corrections applied. For surface waters, prior to analysis, instrument background was recorded, and then samples were purged using the built-in pump in the manifold, isolating it from the HDPE bottle. The sample was then equilibrated (Smith & Swarzenski, 2012), and ^{222}Rn activity was measuring using a continuous 3-hour "sniff test" protocol. Sediment sampling to determine ^{226}Ra-supported ^{222}Rn activity for residence time calculations, ^{224}Ra diffusive flux, and ^{224}Ra desorption are detailed in Text S1 Supporting Information S1. Lastly, concentrations of nitrate + nitrite (method detection limit: 0.1701 µM), orthophosphate (method detection limit: 0.0452 µM), ammonium (method detection limit: 0.2712 µM), and silicate (method detection limit: 0.1709 µM) were measured in accordance with standard protocols and instrument-specific methods using a LACHAT QuikChem® 8500 Series 2 (USEPA, 1993, 1997; Lachat Instruments, 2020).

2.3. Groundwater Residence Times and Reaction Rates

The apparent residence time of subtidal groundwaters was quantified for the Peconic Bay from ^{222}Rn, following Equation 1. Assuming steady-state ^{222}Rn porewater activity with the aquifer sediments (Rn_{eq}), the radon-based residence time was calculated, solving for τ (Tamborski et al., 2017a). The apparent residence time for the Eastern Shore was calculated using only ^{224}Ra of the subtidal groundwaters (^{222}Rn samples not collected) following Equation 2 (Tamborski et al., 2017a),

$$Rn_{pw} = Rn_{eq}\left(1 - e^{-\lambda_{222}\tau}\right) + Rn_{sw}e^{-\lambda\tau} + f_{gw}\left(Rn_{gw}e^{-\lambda\tau}\right) \quad (1)$$

$$\tau = -\frac{1}{\lambda_{224}}\ln\left(1 - \frac{Ra_{pw}}{Ra_{eq}}\right) \quad (2)$$

where Rn_{pw} is the activity of ^{222}Rn in the subtidal groundwater sample, and Rn_{sw} represents the ^{222}Rn activity of the surface water endmember. The freshwater fraction (f_{gw}) represented by each subtidal groundwater sample was calculated using a two-endmember salinity mixing model and the ^{222}Rn activity of the freshest subtidal groundwater (Rn_{gw}) from the December Peconic Bay

sampling event, used for both seasons, with λ_{222} as the ^{222}Rn decay constant (Table S1 in Supporting Information S1). Rn_{eq} represents the secular equilibrium activity of ^{222}Rn with its sediment-bound parent (^{226}Ra), approximated by the highest observed activity in subtidal groundwaters. Two sediment samples collected from the south shore of Great Peconic Bay (December) and were analyzed for equilibrium radon activity following Chanyotha et al. (2014) and additionally analyzed for ^{226}Ra on the RaDeCC to determine the theoretical equilibrium activity (Section 3.4; Table S1 in Supporting Information S1).

Reaction rates within the STE of each embayment were calculated following Wilson et al. (2024a). Nutrient concentrations (C) that follow conservative mixing within the STE were calculated following Equation 3:

$$C = (f_{sw-i} \times C_{sw}) + (f_{gw-i} \times C_{gw}) \quad (3)$$

where f_{sw-i} is the fraction of saline water in a given subtidal groundwater sample, and f_{gw-i} is the fraction of fresh water in the same sample, determined by the salinity of each groundwater sample within the STE (S_i), the salinity of the surface water endmember (S_{sw}), and the salinity of the fresh subtidal groundwater endmember (S_{gw}) (Equation 4, 5).

$$f_{sw-i} = \frac{(S_i - S_{gw})}{(S_{sw} - S_{gw})} \quad (4)$$

$$f_{gw-i} = 1 - f_{sw-i} \quad (5)$$

$$R = \frac{1}{\tau} \int_{low\ salinity}^{high\ salinity} (C_r - C_s)\, dS \quad (6)$$

The net reaction rate, R (μmol m^{-2} d^{-1}), for each nutrient was calculated by integrating the difference between measured subtidal nutrient concentrations (C_r) and predicted conservative mixing concentrations (C_S) across the endmember-defined salinity gradient, normalized by each calculated residence time (τ), following Equation 6. This integration was performed for each site and season to quantify nutrient transformation within the STE from the intertidal and subtidal groundwaters.

3. Results

3.1. Subtidal Groundwater Physicochemical Properties

The Peconic Bay (Summer) groundwater salinity ranged from 2.68 – 29.8, with a mean (± standard deviation) of 26.0 ± 6.87 (n = 19; Figure S1 Supporting Information S1). Surface waters (not shown) were relatively homogenous, averaging 29.3 ± 0.497 (n = 34; Table S2 Supporting Information S1). Redox conditions were variable, ranging from -287 to 181 mV, with most groundwaters being reducing. In winter, subtidal groundwaters were fresher, ranging from 0.15 – 26.6, with an average salinity of 10.6 ± 8.92 (n = 16; Figure S1 Supporting Information S1; Table S2 Supporting Information S1). Winter surface waters were also fresher than summer (27.5 ± 1.04; n = 25). Most subtidal groundwaters were oxic (up to 342 mV), except for four reducing samples collected in Bullhead Bay, with the lowest redox potential at -168 mV. In Peconic Bay, seasonal subtidal groundwater salinity variations suggest that the freshwater-saltwater interface was relatively landward during summer and migrated seaward during winter.

In the Eastern Shore, subtidal groundwater salinity averaged 26.2 ± 6.83 (n = 12; Figure S1 Supporting Information S1; Table S2 Supporting Information S1), with slightly fresher waters observed in the south and one fresher sample collected near the peninsula. The surface waters showed little variation, averaging 29.2 ± 0.368 (n = 21). Most subtidal groundwaters were extremely reducing, with the lowest redox potential at -303 mV, except for one oxic sampled in northern portion of the embayment, in Hog Island Bay (30.0 mV). In the Eastern Shore, moderately reduced groundwater salinities suggest that the confined Yorktown-Eastover aquifer outcrops in portions of the bay.

3.2. Nutrient Distributions

Nutrient concentrations in subtidal groundwaters were generally higher, by up to an order of magnitude or more, than in surface waters (Figure 2; Table S2 Supporting Information S1). There was strong seasonality shown in DIN speciation. The Peconic Bay in August had low subtidal groundwater NO_x (3.89 ± 8.75 µM; mean ± standard deviation hereafter) but relatively higher NH_4 (31.1 ± 45.8 µM). December groundwaters had the highest concentration of NO_x observed between all sampling events (35.2 ± 42.1 µM) and low NH_4 (6.05 ± 12.6 µM), in part reflecting the seasonal migration of the freshwater-saltwater interface. Subtidal groundwater concentrations of PO_4 (4.19 ± 3.73 µM summer vs. 1.43 ± 1.22 µM winter) and DSi (92.1 ± 65.9

328 μM summer vs. 85.0 ± 47.1 μM winter) were slightly higher in the summer than in winter
329 (Figure 2). Surface water DSi concentrations in the summer (56.8 ± 6.95 μM) were notably
330 higher than in winter (7.87 ± 1.47 μM), with elevated concentrations also observed in the
331 Peconic River during summer (96.9 μM vs. 49.8 μM). In contrast, surface water DIN
332 concentrations showed minimal changes between seasons (Table S2 Supporting Information S1).
333 The Eastern Shore (Summer) subtidal groundwaters had much higher NH_4 (105 ± 114 μM), PO_4
334 (16.3 ± 15.5 μM), and DSi (186 ± 173 μM) than the Peconic Bay (Summer).

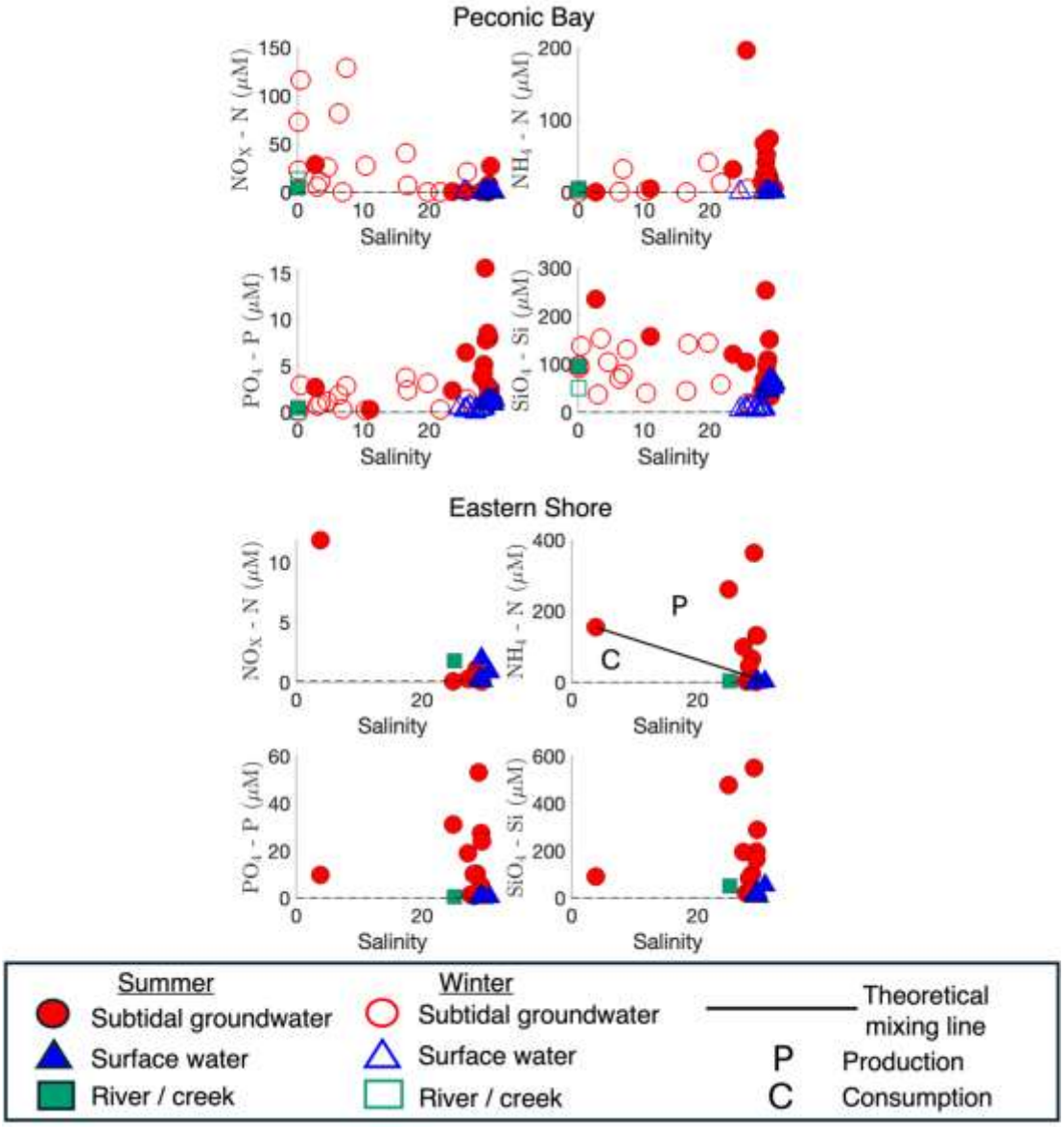

Figure 2. Nutrient concentrations across salinity gradients for all three sites, showing subtidal groundwaters (red circles), surface waters (blue triangles), and river and creeks (green squares). The black line represents the theoretical salinity two-endmember mixing line. The Eastern Shore (right) NH_4 plot shows "P" above a theoretical mixing line indicating production and "C" below the line indicating consumption. Dashed black lines indicate method detection limit.

342 ### 3.3. Radionuclide Distributions

343 The Peconic Bay (Winter) had relatively low surface water radium activities for both
344 ^{224}Ra (11.7 ± 9.65 dpm $100L^{-1}$) and ^{228}Ra (26.4 ± 10.3 dpm $100L^{-1}$; Table S3 Supporting
345 Information S1) compared to the summer (^{224}Ra: 44.5 ± 12.9 dpm $100L^{-1}$; ^{228}Ra: 90.2 ± 15.0
346 dpm $100L^{-1}$). The spatial pattern reversed seasonally, with winter showing depletion towards the
347 west and slight enrichment to the east (Figures 3c and 3d), though elevated activities still existed
348 in Bullhead Bay and along the south shore of Great Peconic Bay. In contrast, the Peconic Bay
349 (Summer) showed depletion in ^{224}Ra and ^{228}Ra toward the east and enrichment toward the west
350 (Figures 3a and 3b), with higher activities near the coastline and hotspots in Bullhead Bay and
351 along the south shore of Noyack Bay. The general depletion of both isotopes towards the east
352 suggests a loss from mixing with the Atlantic Ocean. Although ^{223}Ra was measured, activities
353 were generally low with large uncertainties, and therefore not reported.
354

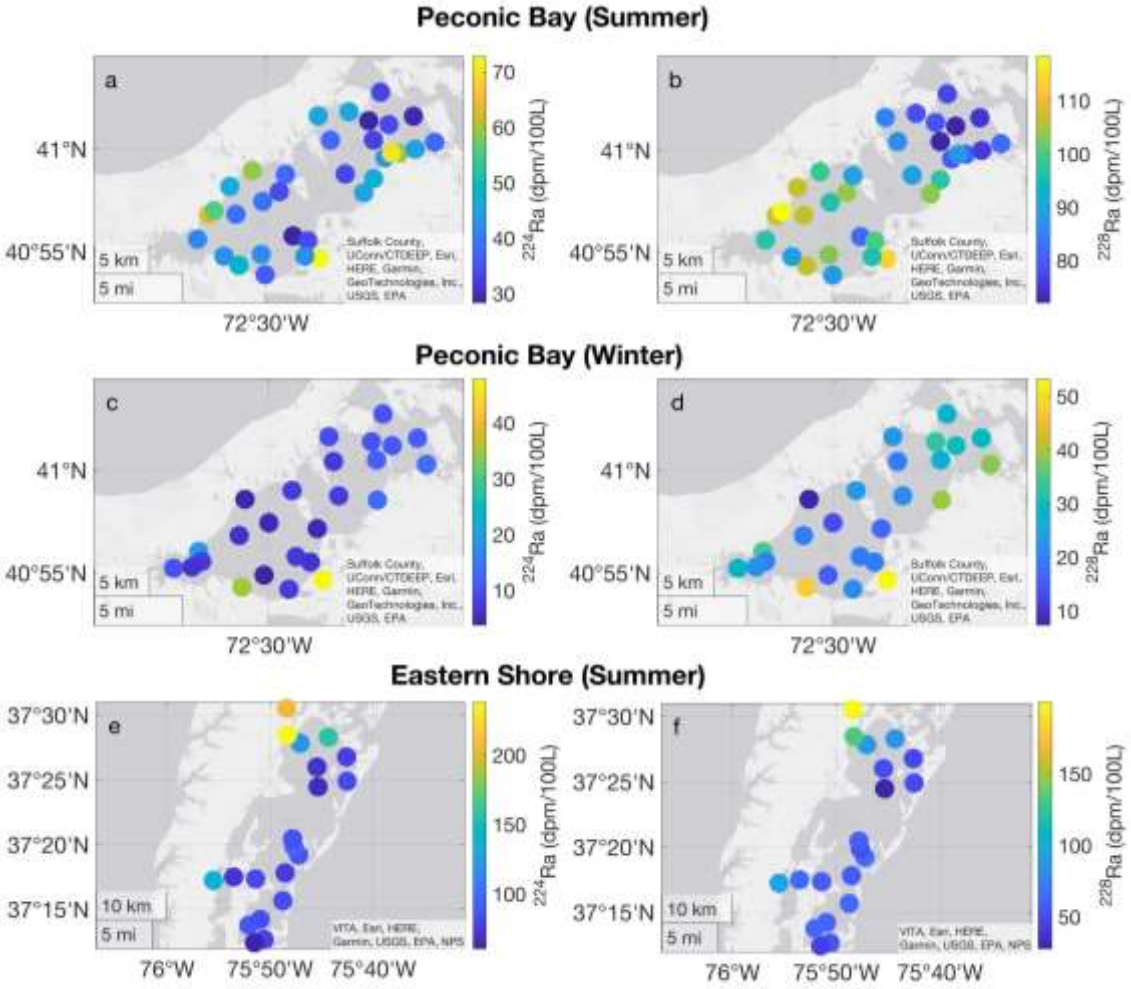

Figure 3. Surface water ^{224}Ra and ^{228}Ra activities in (a, b) Peconic Bay (Summer), (c, d) Peconic Bay (Winter), and (e, f) the Eastern Shore (Summer). Left panels (a, c, e) show ^{224}Ra and right panels (b, d, f) show ^{228}Ra. Note the differences in color bar scales across panels.

The seasonal migration of the freshwater-saltwater interface may explain the low radium activities in winter, as lower salinity reduces radium desorption in the STE. Most of the winter subtidal groundwater samples were fresh (Table S2 Supporting Information S1). Winter subtidal groundwater ^{224}Ra activities averaged 62.8 ± 60.4 dpm 100L^{-1} with ^{228}Ra activities of 23.9 ± 32.0 dpm 100L^{-1}, whereas the summer subtidal groundwater ^{224}Ra activities were 593 ± 353 dpm 100L^{-1} with ^{228}Ra equal to 309 ± 312 dpm 100L^{-1}, more than an order of magnitude higher than winter (Figure 4). However, while the subtidal groundwater and surface water ^{224}Ra and ^{228}Ra activities show drastic seasonal differences, the ^{224}Ra/^{228}Ra activity ratios between the seasons

remain very similar, suggesting the relative contributions of these isotope sources and sinks remain consistent between seasons (Table S3 Supporting Information S1).

In the Eastern Shore, ^{224}Ra and ^{228}Ra show a gradient in Hog Island Bay, with the highest activities along the eastern peninsula coast and lower activities to the west and south (Figures 3e and 3f). Eastern Shore surface waters exhibited relatively higher ^{224}Ra (103 ± 46.3 dpm 100L^{-1}) and ^{228}Ra (70.8 ± 36.6 dpm 100L^{-1}) compared to Peconic Bay, due to its distinct geology and hydrodynamics (Figure 4). While the average subtidal groundwater Ra activities of the two sites look similar for both isotopes (Figure 4), the ^{224}Ra/^{228}Ra activity ratios of the subtidal groundwaters, surface waters, and rivers/creeks show significant variation (Table S3 Supporting Information S1), indicating that the relative sources and sinks of radium vary between sites.

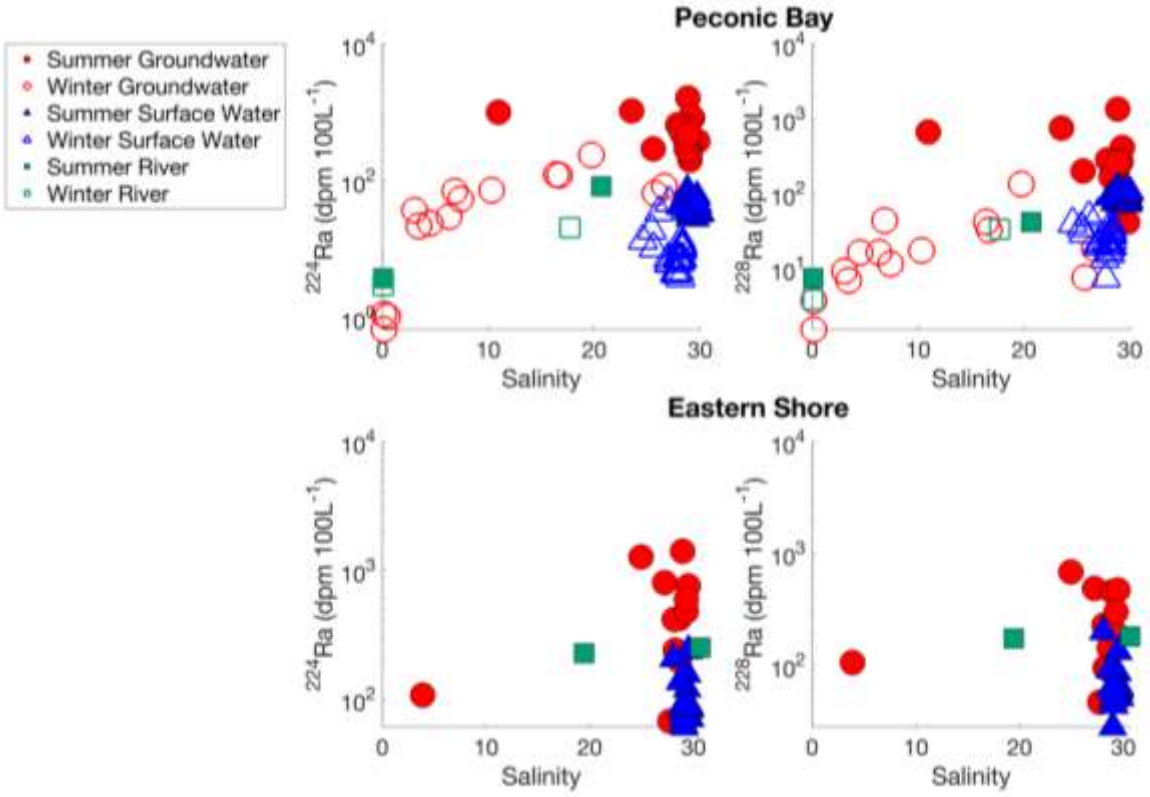

Figure 4. ^{224}Ra activity (left) and ^{228}Ra activity (right) versus salinity for all sample types. The top row illustrates seasonal differences between the Peconic Bay samples collected in summer and winter. The bottom row presents the geologic comparison between Eastern Shore (Summer) samples and the Peconic Bay (Summer) above. Error bars are smaller than data points.

3.4. Groundwater Residence Times & Nutrient Reaction Rates

Residence time within the STE influences the concentration and speciation of nutrients delivered to the coastal ocean from SGD (Wilson et al., 2024c). Subtidal groundwater activities of ^{222}Rn in Peconic Bay ranged from 8.91 – 121 dpm L^{-1} in summer and 9.14 – 80.2 dpm L^{-1} in winter, while the equilibrium ^{222}Rn activity is 149 ± 93.4 dpm L^{-1} (Table S1 in Supporting Information S1). The Eastern Shore (Summer) subtidal groundwater ^{224}Ra activities ranged from 67.4 – 1270 dpm $100L^{-1}$ (Table S3 Supporting Information S1) compared to the Ra_{eq} value of 1410 ± 65.6 dpm $100L^{-1}$ (Table S1 Supporting Information S1). The mean (± standard deviation) apparent residence time of subtidal groundwater calculated using ^{222}Rn was 3.8 ± 1.8 days (August) and 1.7 ± 0.7 days (December) for Peconic Bay, and 2.9 ± 0.6 days for the Eastern Shore (June). These reflect the time elapsed since brackish groundwaters mixed with surface waters and do not reflect absolute ages. The calculated ^{224}Ra residence times averaged 2.3 ± 1.4 days in summer and 1.4 ± 1.2 days in winter, but ^{222}Rn was selected as the preferred tracer for the Peconic Bay as it explicitly accounts for mixing between terrestrial groundwater and seawater in a sandy STE (Chen et al., 2025), conditions characteristic of a coarse-grained study site like the Peconic Bay.

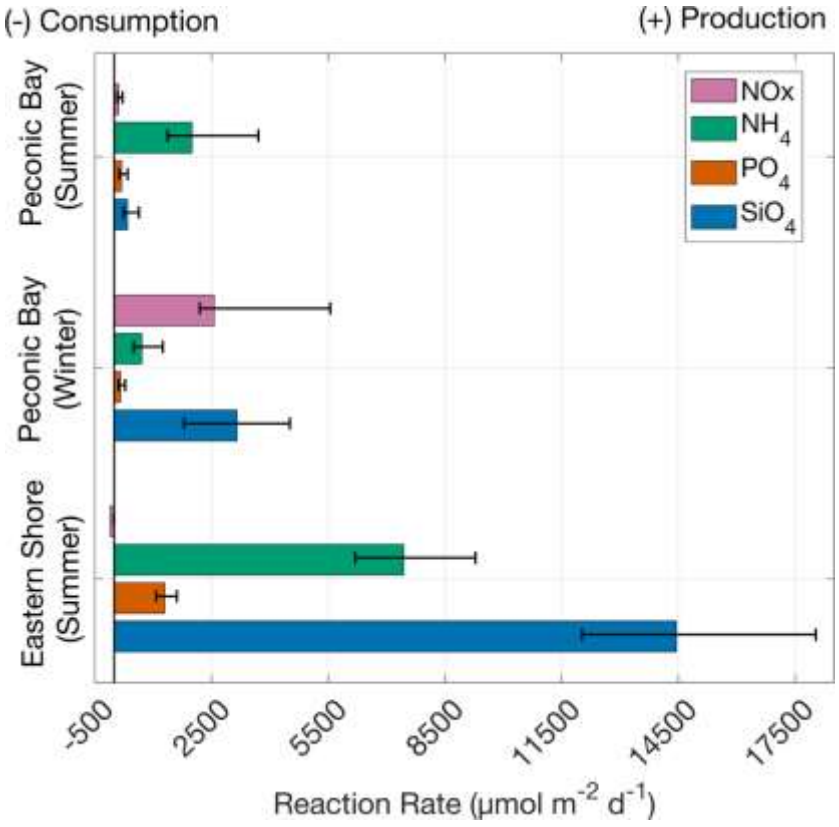

Figure 5. Nutrient reaction rates within each STE. Negative reaction rates (left side) indicate net nutrient consumption, while positive rates (right side) indicate net nutrient production.

Integrating all nutrient deviations along a theoretical conservative mixing line for each STE (Figure 2) allowed for the calculation of net nutrient transformations of NO_x, NH_4, PO_4, and DSi (μmol m^{-2} d^{-1}) to be quantified following Equation 6, adapted from Wilson et al. (2024a). All nutrients for all sites exhibited rates of net production, except for NO_x in the Eastern Shore (Summer) STE, which showed a net consumption (Figure 5). For the Peconic Bay, the highest rate of production found in the summer was for NH_4, at 2.00 x 10^3 (min – max = 1.37 – 3.70 x 10^3) μmol m^{-2} d^{-1}, with lower net production of NO_x, PO_4 and DSi (<500 μmol m^{-2} d^{-1} on average). During the winter, net production rates were dominated by DSi at 3.16 x 10^3 (2.23 – 5.55 x 10^3) μmol m^{-2} d^{-1} and by NO_x with 2.57 x 10^3 (1.81 – 4.51 x 10^3) μmol m^{-2} d^{-1}, up to an order of magnitude greater than during the summer (Figure 5). Phosphate production during the summer was 186 (127 – 344) μmol m^{-2} d^{-1}, nearly identical to winter values of 159 (111 – 279) μmol m^{-2} d^{-1}, suggesting minimal seasonal variation. The Eastern Shore (Summer) exhibited the highest production rates of NH_4, PO_4, and DSi among all sites and seasons (Figure 5). In

contrast, NO_x was the only nutrient found to show net consumption, a rate of -12.1 (-10.1 – -15.2) μmol m^{-2} d^{-1}. Ammonium production in the Eastern Shore was 7.44 x 10^3 (6.19 – 9.29 x 10^3) μmol m^{-2} d^{-1}, PO_4 from 1.29 x 10^3 (1.08 – 1.61 x 10^3) μmol m^{-2} d^{-1}, and DSi of 1.45 x 10^4 (1.20 – 1.80 x 10^4) μmol m^{-2} d^{-1}.

4. Discussion

4.1. Radium Mass Balances

The short half-life ($t_{1/2}$ = 3.6 d) and fast regeneration time of ^{224}Ra make it a useful tracer for short and long PEX and SGD flow paths (Garcia-Orellana et al., 2021). Thus, a ^{224}Ra mass balance is developed to quantify a flux of both TSGD (FSGD + MSGD) and PEX. The ^{228}Ra mass balance, used to trace long flow paths, is used exclusively to quantify the flux of TSGD (Rodellas et al., 2017). The difference between the two mass balances allows for the exclusive quantification of the PEX water flux for each site and season.

Sources of radium to the embayments consist of river or creek inputs, desorption from fine-grained suspended sediments, molecular diffusion and bioturbation from sediments (and SGD; Table S4 in Supporting Information S1). Sink terms consist of a loss from mixing with the coastal ocean and radioactive decay. The general mass balance is solved for the flux of TSGD and PEX (Equation 7):

$$\left(\frac{^{222i}I_{SW-off}}{\tau_{app}}\right) + \left(^{222i}I_{SW} \cdot \lambda_{22i}\right) = \left(Q_{river} \cdot {}^{22i}A_{river}\right) + \left(F_{diff} \cdot SA_{bay}\right) + \left(S_{sed} \cdot SA_{bay} \cdot {}^{22i}A_{desorb} \cdot K_d\right) + F_{MSGD} \cdot {}^{22i}A_{MSGD} + F_{PEX} \cdot {}^{22i}A_{PEX} \quad (7)$$

There are two radium sink terms used in the mass balances. The first is a loss from mixing with the Atlantic Ocean, which incorporates the radium isotope inventory within the embayment, after removing the Atlantic Ocean endmember activity ($^{22i}I_{SW\text{-}off}$; i = 4 or 8). Inventories (dpm) were calculated using each surface water sample's activity (dpm m^{-3}) multiplied by its water column depth (m), averaged, and then multiplied by the embayment's surface area (SA_{bay}; m^2). Digital elevation models were obtained from Richardson et al. (2024) for the Eastern Shore and from NOAA for the Peconic Bay (National Oceanic and Atmospheric Administration National Geophysical Data Center, 2007) to calculate the surface area (SA_{bay}) and volume of each embayment (V_{bay}; m^3). The ^{224}Ra and ^{228}Ra activity of the Atlantic Ocean in the study regions is approximately 3.7 and 2.79 dpm $100L^{-1}$, respectively (Charette et al., 2012; Table S3 Supporting

Information S1). Additionally, the loss from mixing term incorporates the apparent water age of the embayment (τ_{app}; days). The apparent water age of the Peconic Bay is 39.3 days, averaged from Flanders Bay (55 days), Great Peconic Bay (48 days), Little Peconic Bay (32 days), and Shelter Island Sound (22 days), calculated based on tidal prism volume and exchange rates (Hardy, 1976; Bortman & Niedowski, 1998). The Eastern Shore apparent water ages were much shorter, with an average of 5.5 days between all coastal lagoons in the study region, determined from a hydrodynamic model with a passive tracer to simulate water movement and flushing (Herman et al., 2007). The other sink term is the loss of radium due to decay, which consists of the radium inventory of the surface water ($^{22i}I_{SW}$) and the decay constant of the isotope of interest (λ_{22i}).

Radium sources include rivers, diffusion and bioirrigation from sediments, particle desorption, PEX and SGD. The diffusive flux represents the diffusive and bioirrigation radium inputs from sediments in the subtidal area of each embayment (SA_{bay}). Diffusive fluxes (F_{diff}) for ^{224}Ra for the Peconic Bay (Summer) were estimated using averaged values from three muddy sediment cores and a sandy core collected in nearby Long Island Sound by Garcia-Orellana et al. (2014). These fluxes were weighted to the average surficial sediment composition of Peconic Bay: 80% muddy (1.31×10^8 m^2) and 20% sandy (3.29×10^7 m^2), within a total embayment surface area (SA_{bay}; 1.64×10^8 m^2), which is considered surficially oxic year-round. Assuming colder temperatures reduce bioirrigation in winter, the diffusive flux in Peconic Bay (Winter) was considered to reflect molecular diffusion alone and scaled using the minimum ^{224}Ra flux from Garcia-Orellana et al. (2014) to represent sediment contributions. The Eastern Shore ^{224}Ra diffusive flux was quantified using ^{224}Ra:^{228}Th sediment disequilibria (0 – 4 cm disequilibria depth) and assumed to represent the entire surface area of the embayment (SA_{bay}; Table S4 in Supporting Information S1). The ^{228}Ra summer diffusive flux of both sandy and muddy sediments are an average from sediment core incubations from Long Island Sound (Cochran, 1979; Turekian et al., 1996; Tamborski et al., 2017b) and is used for both the Peconic Bay (Summer) and the Eastern Shore. The sediment diffusive flux of ^{228}Ra during winter was omitted due to the presumed suppression of benthic organisms under colder temperatures. Prior studies have noted that redox migration and diminished benthic fauna can significantly limit ^{228}Ra release in winter (Tamborski et al., 2017b), and some have omitted long-lived Ra diffusion in winter entirely (Rama & Moore, 1996; Beck et al., 2007).

Desorption includes (1) tidal resuspension of sediments and (2) release from riverine particles as they encounter saline waters. The riverine radium flux is calculated as the river or creek discharge (Q_{river}; Table S4 in Supporting Information S1) of the Peconic River (USGS #01304500) or Phillips Creek, the latter of which is scaled to account for all creeks discharging into the Eastern Shore (Stanhope et al., 2009), and $^{22i}A_{river}$ is the radium activity of the river or creek in downstream, saline waters (Table S3 Supporting Information S1). Here we assume that fine-grained sediments are resuspended twice daily due to tidal resuspension. Suspended sediment concentration (S_{sed}) for the Peconic Bay (Summer and Winter) are obtained from Garcia-Orellana et al. (2014), with the "spring" S_{sed} used to represent colder season conditions during winter sampling. For the Eastern Shore, suspended sediment concentration was taken from Luek and Beck (2014), based on measurements in the nearby York River Estuary. Radium distribution coefficients (K_d) from Garcia-Orellana et al. (2014) were applied to both sites, while incubation experiments to determine desorbable radium activity ($^{22i}A_{desorb}$) were used only for the Peconic Bay, in both summer and winter. The product of K_d and $^{22i}A_{desorb}$ provides the sediment activity. The Eastern Shore desorption was quantified from a sediment grab sample (Table S4 in Supporting Information S1). The resuspension of ^{228}Ra was excluded from the mass balances because it regenerates slowly in sediments and contributes very little over short timescales and is intrinsically included in the river fluxes.

Solving the mass balances for the remaining source term yields the SGD-derived tracer flux (dpm d^{-1}). Dividing the ^{228}Ra tracer flux by the ^{228}Ra subtidal groundwater endmember activity ($^{22i}A_{MSGD}$; Table S3 Supporting Information S1) produces a TSGD flux, which includes both brackish and saline components. Because radium desorbs along brackish flow paths due to cationic exchange at higher ionic strength (Garcia-Orellana et al., 2021), FSGD is inherently included in this estimate, assuming complete mixing. To isolate the PEX flux, the TSGD contribution (via ^{228}Ra) is subtracted from the ^{224}Ra-derived tracer flux, after dividing by the radium activity of the PEX endmember ($^{22i}A_{PEX}$; Table S3 Supporting Information S1). This approach provides separate volumetric flux estimates for TSGD and PEX (m^3 d^{-1}), similar to Rodellas et al. (2017).

4.2. Endmember Selection

Well-constrained radium endmembers are critical to accurately quantifying SGD fluxes, as different radium isotopes respond uniquely to various sources and sinks within a mass balance

framework (Tamborski et al., 2020; Text S2 Supporting Information S1). Poorly constrained radium endmember activities can significantly change the resulting volumetric flux of SGD or PEX, with endmember uncertainty often being a primary contributor to overall flux uncertainty (Liu et al., 2025). This becomes particularly important in seasonal comparisons, where unaccounted for seasonal variability in endmember selection can further increase uncertainty (Gonneea et al., 2013). Endmembers for the ^{224}Ra mass balances were selected from subtidal groundwater samples with the highest ^{224}Ra/^{228}Ra activity ratios (Garcia-Orellana et al., 2021; Table S3 Supporting Information) and among the highest salinities at each site and season (Table S2 Supporting Information S1).

Endmembers were identified for the ^{228}Ra mass balances by extrapolating dissolved silicate (DSi) concentrations against ^{228}Ra activity (Figure S2 in Supporting Information S1). Longer-scale groundwater flow paths (MSGD) enrich fluids in DSi due to silicate mineral weathering (Oehler et al., 2019), so an extrapolated theoretical conservative mixing line between low-DSi saline surface waters and high-DSi subtidal groundwaters was used to identify SGD-influenced waters. Subtidal groundwater samples that fell on or near the extrapolated linear regression model of the surface water samples were selected as ^{228}Ra (and nutrient) endmembers, while any samples already used for the ^{224}Ra endmembers were omitted from use. The Peconic Bay (Winter) subtidal groundwaters exhibited exceptionally low ^{228}Ra and ^{224}Ra activities (Table S3 Supporting Information S1), with average salinity values in winter below 11 (Table S2 Supporting Information S1). Average ^{228}Ra activity in subtidal groundwater (23.9 ± 32.0 dpm 100L^{-1}) was lower than in surface waters (26.4 ± 10.3 dpm 100 L^{-1}). Consequently, the DSi-^{228}Ra theoretical mixing line was not applied for the winter; instead, two subtidal groundwaters with higher salinities (19 and 16) and negative ORP were selected (Table S2 Supporting Information S1), as they had the highest ^{228}Ra subtidal groundwater activities observed in winter (Table S3 Supporting Information S1).

The same subtidal groundwater endmembers selected for radium mass balance calculations were also used as nutrient endmembers (Table S5 in Supporting Information S1) to estimate PEX and MSGD nutrient fluxes, with MSGD nutrient fluxes calculated as TSGD nutrient flux corrected for FSGD nutrient contributions. Similarly, the surface water endmembers used in reaction rate calculations were applied as surface water nutrient endmembers (Table S5 in Supporting Information S1) for each respective flux. FSGD endmembers were defined as the

subtidal groundwater samples with the lowest salinities observed during each field campaign (n = 1 per site and season): 2.86 for Peconic Bay (Summer), 0.15 for Peconic Bay (Winter), and 3.89 for the Eastern Shore (Summer).

4.3. Quantifying FSGD, MSGD, and PEX Water Flux

The FSGD flux for the Peconic Bay was derived from a U.S. Geological Survey groundwater model that replicates fresh groundwater flow in the aquifer system on Long Island, constrained to the Peconic Bay area under consideration (1.98×10^5 m^3 d^{-1}; Jahn & Walter, 2025). This annual FSGD flux was used to represent both seasons. The total freshwater flux to the Eastern Shore (summer) is estimated from Chincoteague Bay, a similarly sized embayment just north of the coastal lagoons of this study in the Delmarva Peninsula. The absolute groundwater flux to Chincoteague Bay is 4.39×10^4 m^3 d^{-1} (Dillow & Greene, 1999) over an area of 5.25×10^7 m^2, calculated using a water balance approach incorporating regional precipitation and evaporation data, assuming the water table is in steady-state. This water flux to the Eastern Shore was then scaled to the area of the embayment, resulting in a freshwater flux of 2.11×10^5 m^3 d^{-1}. The FSGD water flux was subtracted from the TSGD flux from the ^{228}Ra mass balance, allowing for the isolation of MSGD, as it is very unlikely that FSGD bypasses this brackish interface before discharging into the embayments. Uncertainties were calculated using standard error propagation methods, assuming independence of variables; however, there was no error associated with the FSGD water fluxes derived from Jahn & Walter (2025) or Dillow & Greene (1999).

The dominant water flux of the Peconic Bay (Summer) was from PEX ($4.87 \pm 3.30 \times 10^6$ m^3 d^{-1}; 2.96 ± 2.01 cm d^{-1}), followed by MSGD ($2.38 \pm 2.37 \times 10^6$ m^3 d^{-1}; 1.45 ± 1.38 cm d^{-1}), and FSGD (0.199×10^6 m^3 d^{-1}), where the FSGD only represents ~3% of the total SGD flux to the embayment. During the winter, the MSGD water flux ($5.60 \pm 3.57 \times 10^6$ m^3 d^{-1}; 3.41 ± 2.17 cm d^{-1}) was slightly higher than PEX ($4.56 \pm 3.62 \times 10^6$ m^3 d^{-1}; 2.77 ± 2.20 cm d^{-1}; Figure S3 Supporting Information S1) potentially indicating a seasonal shift in long-scale groundwater flow dynamics due to migration of the freshwater-saltwater interface. The Eastern Shore (Summer) also saw the opposite water flux pattern as the Peconic Bay (Summer), with a much higher MSGD flux ($10.4 \pm 6.58 \times 10^6$ m^3 d^{-1}; 4.20 ± 2.59 cm d^{-1}) than PEX ($2.06 \pm 1.20 \times 10^6$ m^3 d^{-1}; 0.82 ± 0.48 cm d^{-1}), and the FSGD representing less than 2% of the total water flux (Figure S3 Supporting Information S1). These differences in dominant water fluxes are likely driven by

contrasting surficial geology, with the coarse-grained glacial sediments underlying the Peconic Bay favoring PEX, whereas the fine-grained surficial sediments of the Eastern Shore partially restrict PEX, resulting in a relatively greater contribution from MSGD.

The Peconic Bay MSGD flux exhibits strong seasonality, while the PEX flux remains constant between seasons (Figure S3 Supporting Information S1). Seasonal variations in MSGD are driven by the seasonal exchange of seawater as the as the freshwater-saltwater interface migrates (Michael et al., 2005), as evidenced by the extremely low salinities observed in the subtidal groundwater samples collected in December. This interface can commonly migrate due to the seasonal variations in aquifer recharge or fluctuations in sea level (Santos et al., 2012). The reduction of pumping during winter (Stumm et al., 2024) and increase in precipitation coupled with the reduction of evapotranspiration during colder months increases the hydraulic head of the surficial aquifer, allowing for increased water flux through the brackish to saline interface (Schubert, 1998). During wet periods or reduced municipal pumping, the water table rises, shifting the freshwater-saltwater interface seaward and flushing previously intruded seawater back to the embayment (Michael et al., 2005; Santos et al., 2012). This expansion of the freshwater lens compresses and displaces saline water. Even small rises in the water table from recharge can drive substantial interface movement, as the Ghyben-Herzberg relationship predicts a ~40:1 depth ratio (Xun & Ying, 2009).

The surficial fine-grained lagoon sediments in the Eastern Shore may limit the depth and magnitude of PEX. Grain size acts as a key physical control on both SGD and PEX and the depth to which surface waters can penetrate sediments (Hartl, 2006). Sediment permeability largely governs water circulation (Santos et al., 2012), with fine-grained sediments, like those found surficially in the Eastern Shore, often showing hydraulic conductivities one to two orders of magnitude lower than coarser sands (Richardson, 1994). This lower permeability restricts exchange to shallower depths, inhibiting rapid circulation as PEX. Beneath these fine-grained layers, however, lies the highly permeable Yorktown-Eastover aquifer, which can exhibit horizontal hydraulic conductivity values as high as 1570 cm d^{-1} (Richardson, 1994). These deeper, more permeable layers likely facilitate large-scale, deeper MSGD fluxes in the Eastern Shore region, while PEX remains constrained by the surficial sediment texture. However, potential geologic heterogeneity, such as potential outcropping of the confined Yorktown-Eastover aquifer, and biologically-mediated conduits like seagrass roots and bioirrigation may

create alternative pathways that allow deeper groundwater to move through the low-permeability cap and discharge to the embayment.

4.4. Nutrient Pathways

To account for mixing with overlying surface water and its inherent recirculation within the STE (Cook et al., 2018; Wilson et al., 2024b), surface water nutrient concentrations were subtracted from subtidal groundwater endmember concentrations in the PEX and MSGD flux calculations. The FSGD-derived nutrient flux, however, needs to be modified; as it passes through the subterranean estuary, nonconservative species are altered (Santos et al., 2009), so a correction term (M) needs to be applied to reflect net nutrient transformations of reduction ($M < 0$) or production ($M > 0$) (Equation 8) following Wilson et al. (2024b), where $[C]_{observ.}$ represents the summed total of the in situ measured nutrient concentrations and $[C]_{conserv.}$ represents the summed total of the conservative nutrient concentrations predicted along the theoretical salinity mixing model (Figure 2). The correction term is then applied to the fresh groundwater endmember nutrient concentrations ($[C_{fgw}]$; Table S5 in Supporting Information S1), resulting in a corrected nutrient concentration ($[C]_M$) to be used to quantify the FSGD-nutrient derived fluxes (Equation 9).

$$M = \frac{[C]_{observ.} - [C]_{conserv.}}{[C]_{conserv.}} \quad (8)$$

$$[C]_M = \left(M \times [C_{fgw}]\right) + [C_{fgw}] \quad (9)$$

In Peconic Bay, MSGD dominated N delivery in summer, exporting orders of magnitude more NH_4 ($9.64 \pm 9.20 \times 10^2$ µmol m^{-2} d^{-1}) than NO_x (1.45 ± 1.38 µmol m^{-2} d^{-1}) (Figure 6). In winter, NH_4 and NO_x via MSGD were comparable ($7.01 \pm 4.47 \times 10^2$ µmol NH_4 m^{-2} d^{-1}; $6.97 \pm 4.44 \times 10^2$ µmol NO_x m^{-2} d^{-1}), consistent with seasonal redox shifts in the STE. PEX also shifted from NH_4-rich in summer ($6.40 \pm 4.34 \times 10^2$ µmol m^{-2} d^{-1}) to NO_x-rich in winter ($3.86 \pm 3.06 \times 10^2$ µmol m^{-2} d^{-1}). For PO_4, MSGD was the primary pathway in both seasons (74.1 ± 70.7 µmol m^{-2} d^{-1} in summer; $1.03 \times 10^2 \pm 65.4$ µmol m^{-2} d^{-1} in winter), although the summer PEX-driven PO_4 flux (53.7 ± 36.4 µmol m^{-2} d^{-1}) closely followed that supplied by MSGD. Notably, the lowest flux observed was PO_4 via FSGD in winter (1.08 µmol m^{-2} d^{-1}). DSi fluxes supplied in winter via MSGD ($2.93 \pm 1.87 \times 10^3$ µmol m^{-2} d^{-1}) and PEX ($12.5 \pm 9.9 \times 10^2$ µmol m^{-2} d^{-1}) were

higher than in summer (MSGD: 7.67 ± 7.33 x 10^2 µmol m^{-2} d^{-1}; PEX: 4.46 ± 3.02 x 10^2 µmol m^{-2} d^{-1}), while the summer DSi FSGD flux (3.07 x 10^2 µmol m^{-2} d^{-1}) was higher than in winter (1.55 x 10^2 µmol m^{-2} d^{-1}). Overall, MSGD was the dominant DSi pathway across both seasons (Figure 6).

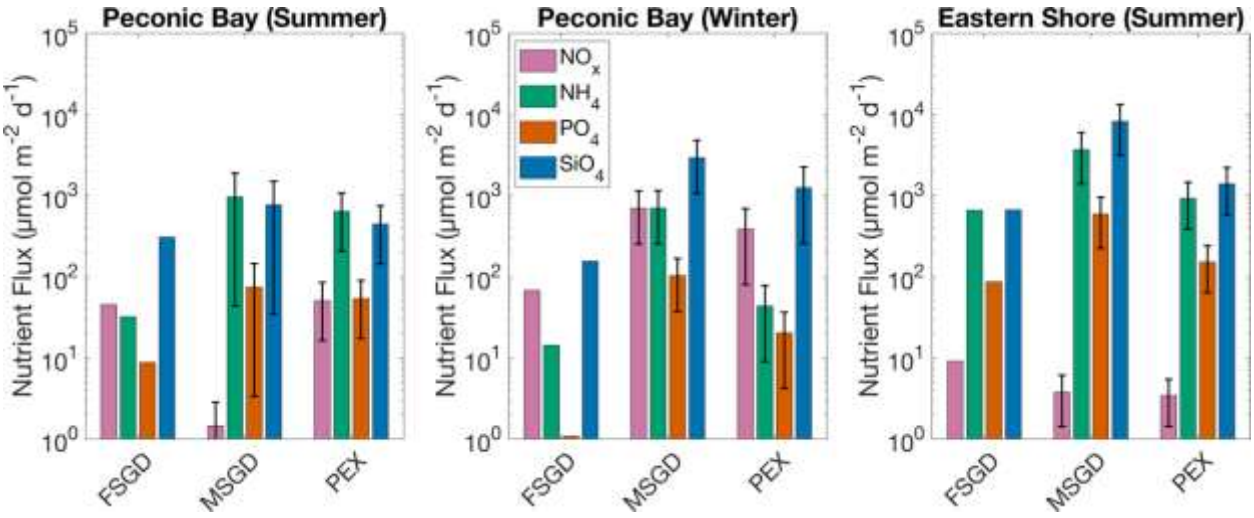

Figure 6. Area-normalized nutrient fluxes, by pathway. FSGD refers to fresh submarine groundwater discharge; MSGD refers to marine (saline) submarine groundwater discharge; PEX refers to pore water exchange.

Both sites in the summer showed NH_4 via MSGD dominated N export by orders of magnitude (Eastern Shore: 3.68 ± 2.28 x 10^3 µmol NH_4 m^{-2} d^{-1}; 3.77 ± 2.33 µmol NO_x m^{-2} d^{-1}). PEX in the Eastern Shore also supplied much higher NH_4 fluxes (9.25 ± 5.39 x 10^2 µmol m^{-2} d^{-1}) over NO_x (3.44 ± 2.01 µmol m^{-2} d^{-1}), as did the Peconic Bay (50.6 ± 34.3 µmol NO_x m^{-2} d^{-1}). For both PO_4 and DSi at both sites, the highest nutrient fluxes were delivered by MSGD, followed by PEX, with the Eastern Shore MSGD delivering larger nutrient fluxes than the Peconic Bay overall (Figure 6). The Eastern Shore MSGD PO_4 flux (5.89 ± 3.65 x 10^2 µmol m^{-2} d^{-1}) was slightly higher than that supplied by PEX (1.52 x 10^2 ± 8.87 x 10^1 µmol m^{-2} d^{-1}), with the PO_4 flux via FSGD following closely behind (86.4 µmol m^{-2} d^{-1}). The MSGD-supplied DSi flux to the Eastern Shore (8.23 ± 5.10 x 10^3 µmol m^{-2} d^{-1}) was the largest nutrient flux observed overall between both sites and seasons. Overall, MSGD supplied the largest NH_4, PO_4, and DSi loads to both embayments during the summer even though PEX was the dominant water flux to the

660 Peconic Bay (Summer) while FSGD, despite its small water flux contributions to both
661 embayments, disproportionately contributed NO_x.
662

663 ### 4.5. Nutrient Transformations

664 Seasonal shifts in Peconic Bay nutrient transformations within the STE drive variability
665 in nutrient fluxes. In summer, NH_4 production within the STE was nearly an order of magnitude
666 greater than NO_x (Figure 5), suggesting active organic matter mineralization (Wilson et al.,
667 2023), microbial denitrification, and/or dissimilatory nitrate reduction to ammonium (DNRA)
668 (Addy et al., 2005; Wilson et al., 2023). The winter seaward migration of the freshwater-
669 saltwater interface enhances deeper oxygen penetration within the STE (Moore & Joye, 2021),
670 potentially promoting nitrification. This likely explains the elevated winter NO_x production
671 (Figure 5) and consistently higher NO_x flux than NH_4 flux across all pathways during winter
672 (Figure 6). In contrast, phosphate production showed little seasonal variation (Figure 5), though
673 the PO_4 flux via FSGD was lower in winter than in summer (Figure 6). More oxic conditions
674 along the FSGD flow path in winter enhance sorption of phosphate onto Fe/Mn oxides, while
675 summer's more reducing conditions promote desorption from Fe/Mn oxides (Charette &
676 Sholkovitz, 2002). Lastly, winter showed increased MSGD and associated DSi fluxes, likely due
677 to either the enhanced flow rates or enhanced silicate weathering along the deeper, older flow
678 paths (Oehler et al., 2019).

679 Nutrient fluxes within the Eastern Shore STE are strongly shaped by its fine-grained,
680 clay-rich surficial sediments, which limits oxygen penetration and promotes strongly reducing
681 conditions. This geology supports an environment conducive to denitrification, as evidenced by
682 the net consumption of NO_x (Figure 5) and elevated NH_4 fluxes across all flow paths, which are
683 over two orders of magnitude higher than NO_x (Figure 6). This contrasts with Peconic Bay
684 (Summer), where NO_x FSGD fluxes are more dominant, and NO_x was moderately produced
685 (Figure 5). The Eastern Shore also exhibited the highest PO_4 production rate in the STE, likely
686 driven by desorption from Fe/Mn oxides under strongly reducing conditions, increased organic
687 matter remineralization, or a land-usage signal such as nearby poultry-processing facilities to the
688 north of the embayment (Environmental Integrity Project, 2020). Additionally, DSi production
689 and flux was highest in the Eastern Shore, possibly enhanced by silicate mineral dissolution in
690 muddy, clay-rich sediments and/or diatom dissolution (Zhu et al., 2024). While residence times

691 within the STE influence the concentration and speciation of nutrients delivered to the coastal
692 ocean from SGD (Wilson et al., 2024c) groundwater residence times were comparable between
693 the Eastern Shore (2.9 ± 0.6) and Peconic Bay (Summer) (3.9 ± 1.8), indicating that the observed
694 differences in nutrient production are governed by the underlying geologic differences and
695 nutrient sources, and less dependent on the time spent interacting with the STE sediment matrix.
696 Nutrient production rates are lower than the nutrient fluxes delivered by MSGD, on a per
697 unit area basis, assuming the STE spans the entire embayment surface area. This suggests that
698 nutrients are not only produced or consumed in situ but are also remineralized, transformed, and
699 transported along deeper groundwater flow paths, which ultimately contributes to excess nutrient
700 loading into the embayment. The variation between the calculated reaction rates and nutrient
701 fluxes indicates that nutrient cycling in these systems is not tightly coupled, but instead MSGD
702 mobilizes nutrients that have been both newly produced and previously stored within the aquifer
703 matrix and/or sourced from the terrestrial upland (Santos et al., 2021). Integrating STE-based
704 reaction rates with mass balance nutrient loading estimates offers a more complete picture of
705 nutrient dynamics, and shows that coastal nutrient availability is driven not only by internal
706 cycling, but also by flow paths that deliver and rework nutrients from differing biogeochemical
707 sources.

708 ### 4.6. Comparing DIN Loads to Embayments

709 Dissolved inorganic nitrogen (DIN; NO_x + NH_4) fluxes supplied via FSGD and MSGD
710 for each season and site were respectively combined to represent a TSGD flux. These fluxes
711 were compared to known absolute DIN loads supplied by the Peconic River to the Peconic Bay
712 and atmospheric deposition of nitrogen for Suffolk County (Monti et al., 2024), where Peconic
713 Bay is located, and scaled to the bay surface area. Absolute DIN loads to the Eastern Shore
714 include baseflow-supplied creek discharge (Stanhope et al., 2009) and atmospheric deposition of
715 nitrogen (Brush et al. 2015a,b). The DIN loads supplied by TSGD and PEX are greater than the
716 DIN supplied by atmospheric deposition, and by rivers or creeks to both embayments (Figure S4
717 Supporting Information S1), highlighting the need for more consideration of SGD and PEX in
718 coastal nutrient budgets.
719 Nitrogen total maximum daily loads (TMDLs) for the Peconic Bay are separated by
720 source (atmospheric deposition, meteoric groundwater, small tributaries, stormwater), and by
721 season (Peconic Estuary Partnership, 2007). Here, individual bay N-TMDLs (Flanders Bay,

Great Peconic Bay, and Little Peconic Bay) are seasonally combined to represent a total TMDL for the same total region presented in this study. Noyack Bay does not have a stand-alone TMDL and is excluded from these regulatory totals. The resulting summed nitrogen totals are 9.45 x 10^5 mol d^{-1} for summer and 6.29 x 10^5 mol d^{-1} for winter. Total DIN loads supplied to the Peconic Bay in summer by TSGD are 1.72 ± 1.50 x 10^5 mol d^{-1} and 2.43 ± 1.03 x 10^5 in winter, equivalent to 18.2% in summer and 38.7% of the total nitrogen TMDL budgets to the embayments, respectively. These percentages may be inflated because the regulatory TMDL totals exclude Noyack Bay and, conversely, may be deflated because the TMDLs are for total nitrogen (DIN + organic N) while our fluxes only consider inorganic N, and without including PEX-derived DIN loads. Considering these uncertainties, our results still demonstrate that SGD is a critical contributor of nitrogen to the Peconic Bay and should be considered in its coastal nutrient budget to expand beyond meteoric, fresh groundwater.

Margalefidinium polykrikoides (formerly *Cochlodinium*; Gómez et al., 2017) is a bloom-forming dinoflagellate that typically proliferates in late summer. It has been linked to significant fish and shellfish mortality in the Peconic Estuary and the lower Chesapeake Bay of Virginia (Gobler et al., 2012; Mulholland et al., 2009). This species is notable for its ability to rapidly assimilate both organic and inorganic nitrogen forms (Gobler et al., 2012). Assuming a well-mixed Peconic Bay (volume = 9.43 x 10^{11} L), the combined NH_4 supplied from TSGD and PEX into the entire bay yields a daily concentration of 0.279 ± 0.177 µmol L^{-1} d^{-1}. When compared to the ammonium concentration required to sustain the NH_4-based growth rate of *M. polykrikoides* (0.44 ± 0.02 d^{-1}; Gobler et al., 2012), which corresponds to a half-saturation constant (K_s) of 2.69 ± 0.49 µM, this supply accounts for 10.4% ± 6.85% of the species' daily ammonium demand. With an average apparent water age of the entire embayment of 39.3 days (Hardy, 1976; Bortman & Niedowski, 1998), and neglecting any additional updake or flushing, the TSGD+PEX NH_4 flux alone could supply a bloom within just 9.6 days in Peconic Bay.

No nitrogen or phosphorus TMDLs are currently established for the seaside coastal embayments of the Eastern Shore (Virginia Department of Environmental Quality, 2021). In contrast, several Chesapeake Bay-side watersheds on the Eastern Shore have TMDLs for total nitrogen, total phosphorus, and total suspended solids. Applying the same NH_4-driven growth rate and K_s for *M. polykrikoides* used above, the combined NH_4 input from TSGD and PEX to the Eastern Shore is 1.16 ± 0.59 x 10^{12} µmol d^{-1}. Distributed over the entire embayment volume

753 (3.03×10^{11} L), this supply can meet 142 ± 77% of the daily NH_4 requirement for *M.*
754 *polykrikoides*, indicating SGD and PEX-derived NH_4 alone can sustain a bloom. However,
755 limited algal blooms are reported within the embayment, possibly due to the rapid flushing of the
756 coastal lagoons with the Atlantic (5.5 days; Herman et al., 2007), or other limiting controls (light
757 limitations, co-nutrient availability, grazing). Regardless, the high NH_4 fluxes and strong STE
758 NH_4 production on the Eastern Shore are large enough to potentially initiate blooms, and because
759 SGD is typically overlooked in budgeting, its role in periodic eutrophication may be
760 underestimated.

761 ## 5. Conclusions

762 Nutrient loading to coastal embayments is governed by the water flux of different SGD
763 and PEX pathways, as well as nutrient reaction rates within the STE. By coupling reaction rates
764 to mass balance flux estimates, we distinguish between FSGD and MSGD from PEX, quantify
765 their water and nutrient fluxes, and account for transformations that modify FSGD as it transits
766 the STE. This integrated framework reveals how seasonality and permeability regulate nutrient
767 production/consumption and transport to explain site-specific differences in nutrient loading.
768 These results provide a more complete accounting of SGD and PEX-derived nutrients to be used
769 in coastal nutrient budgets to better inform coastal nutrient management issues, such as TMDL
770 limits or the potential to supply algae blooms.

771 Overall, the nutrient fluxes appear to be linked to sediment permeability, which controls
772 both water exchange rates and oxygen penetration depth. In the highly permeable glacial
773 sediments of Peconic Bay, PEX dominated during the summer with little seasonal variability.
774 However, in winter, MSGD increased, likely due to the seaward migration of the freshwater-
775 saltwater interface. This migration was likely able to occur rapidly because of the high
776 permeability of the glacial aquifer, which allows the interface to respond quickly to changes in
777 recharge with minimal lag time. The oxic conditions of the surficial sediments year-round
778 promoted net NO_x production and nitrification, even in summer. Winter conditions likely
779 enhanced PO_4 sorption onto Fe/Mn oxides, while summer's more reducing conditions favored
780 higher PO_4 fluxes. Increased winter MSGD also corresponded with higher DSi fluxes, likely
781 from enhanced silicate mineral weathering from deeper, longer-scale flow paths.

782 In contrast, the lower permeability, fine-grained surficial sediments of the Eastern Shore
783 likely restricted PEX and oxygen penetration depth but permitted a high MSGD flux due to the

high hydraulic conductivity of the underlying sandy aquifer, hinting at geologic heterogeneity and biological conduits as providing pathways through the surface layer. This strongly reducing environment promoted denitrification, reflected by a net NO_x consumption rate and elevated NH_4. This site also showed the highest PO_4 and DSi production, likely driven by Fe/Mn oxide desorption and weathering of clay-rich silicate minerals and/or buried diatom dissolution. Further investigations should consider a seasonal comparison of the Eastern Shore to explore variability in water fluxes and redox-sensitive nutrient transformations.

While FSGD accounted for 3% or less of the total water flux to both sites, it is a significant contributor of nutrients to the coastal embayments and should not be overlooked. Importantly, residence times in the subterranean estuary were similar across sites and seasons, indicating that differences in nutrient fluxes stem from hydrogeologically-mediated redox controls, not water-rock interaction time. Across both sites and seasons, groundwater-derived nitrogen fluxes exceed those from rivers, creeks, and atmospheric deposition and have the potential to supply algae blooms. These findings highlight the significance of both geologic and seasonal variability in regulating the magnitude and transformations driving speciation of SGD-derived nutrient fluxes to coastal systems.

Acknowledgments

This project has been funded wholly or in part by the United States Environmental Protection Agency under cooperative agreement 83967501 to Restore America's Estuaries. The contents of this document do not necessarily reflect the views and policies of the Environmental Protection Agency, nor does the EPA endorse trade names or recommend the use of commercial products mentioned in this document. For more information, please see https://estuaries.org/initiatives/watershedgrants/. We thank everyone in the Old Dominion University Coastal Tracers Lab for their help with field work and radium analyses. Also, thanks to our boat captains, Mark Long and Shawn Droskoski of Suffolk County Department of Health Services, and Sophia Hoffman at the VCLTER.

Conflict of Interest Disclosure

The authors declare there are no conflicts of interest for this manuscript.

Data Availability Statement

The data featured in this manuscript are publicly available through Hydroshare. Physicochemical, radionuclide, and biogeochemical data for the Peconic Bay (both seasons) can be accessed at https://doi.org/10.4211/hs.821a185b2b0b4f8eb920102d1a93171d, and the corresponding data for the Eastern Shore are available at https://doi.org/10.4211/hs.a36c7009ee784d10a23c135b56ee5691.

References

Addy, K., Gold, A. J., Nowicki, B. L., McKenna, J., Stolt, M., & Groffman, P. M. (2005). Denitrification capacity in a subterranean estuary below a Rhode Island fringing salt marsh. *Estuaries, 28(6)*, 896–908. https://doi.org/10.1007/BF02696018

Beck, A., Rapaglia, J., Cochran, J., & Bokuniewicz, H. (2007). Radium mass-balance in Jamaica Bay, NY: Evidence for a substantial flux of submarine groundwater. *Marine Chemistry*, *106(3–4)*, 419–441. http://dx.doi.org/10.1016/j.marchem.2007.03.008

Bortman, M., & Niedowski, N. (1998). *Characterization Report of the Living Resources of the Peconic Estuary*. Riverhead: Peconic Estuary Program, Suffolk County Department of Health Services. Retrieved from https://www.peconicestuary.org/wp-content/uploads/2017/06/CharacterizationReportoftheLivi.pdf

Brandes, J. A., Devol, A. H., & Deutsch, C. (2007). New developments in the marine nitrogen cycle. *Chemical Reviews*, *107(2)*, 577–589. https://doi.org/10.1021/cr050377t

841 Brush, M. J., Harris, L. A., Giordano, J. C. P., & York, J. K. (2015a). *Delmarva coastal bays*
842 *nitrogen loading model: User's guide and documentation*. Virginia Institute of Marine Science.
843 Retrieved from: https://www.vims.edu/people/brush_mj/pubs/CoastBay_NLM_AUG15.pdf
844
845 Brush, M. J., Harris, L. A., Giordano, J. C. P., & York, J. K. (2015b). *Delmarva Coastal Bays*
846 *Nitrogen Loading Model*. [Data set]. Virginia Institute of Marine Science. Retrieved from:
847 https://www.vims.edu/research/units/labgroups/semp/models/
848
849 Burnett, W. C., & Dulaiova, H. (2003). Estimating the dynamics of groundwater input into the
850 coastal zone via continuous radon-222 measurements. Journal of Environmental Radioactivity,
851 *69(1–2),* 21–35. https://doi.org/10.1016/S0265-931X(03)00084-5
852
853 Cai, P., Shi, X., Moore, W. S., & Dai, M. (2012). Measurement of 224Ra:228Th disequilibrium
854 in coastal sediments using a delayed coincidence counter. *Marine Chemistry*, *138–139*, 1–6.
855 https://doi.org/10.1016/j.marchem.2012.05.004
856
857 Chanyotha, S., Kranrod, C., & Burnett, W. C. (2014). Assessing diffusive fluxes and pore water
858 radon activities via a single automated experiment. *Journal of Radioanalytical and Nuclear*
859 *Chemistry*, *301(2)*, 581–588. https://doi.org/10.1007/s10967-014-3157-3
860
861 Charette, M. A., & Allen, M. C. (2006). Precision ground water sampling in coastal aquifers
862 using a direct-push, shielded-screen well-point system. *Groundwater Monitoring and*
863 *Remediation, 26(2)*, 87–93. https://doi.org/10.1111/j.1745-6592.2006.00076.x
864
865 Charette, M. A., W. S. Moore, and W. C. Burnett (2008), Uranium- and thorium-series nuclides
866 as tracers of submarine groundwater discharge. In S. Krishnaswami and J. K. Cochran (Eds.),
867 *Radioactivity in the Environment* (Vol. 13, pp. 155–191). Amsterdam, Elsevier.
868 https://doi.org/10.1016/S1569-4860(07)00005-8.
869
870 Charette, M. A., Dulaiova, H., Gonneea, M. E., Henderson, P. B., Moore, W. S., Scholten, J. C.,
871 & Pham, M. K. (2012). GEOTRACES radium isotopes interlaboratory comparison experiment.

Limnology and Oceanography: Methods, *10*(*6)*, 451–463.
https://doi.org/10.4319/lom.2012.10.451

Chen, X., Santos, I. R., Du, J., Xu, B., Tamborski, J. J., He, D., et al. (2025). Sandy subterranean estuaries minimize groundwater nitrogen pollution impacts on coastal waters. *Geophysical Research Letters*, *52(3),* 1-12. https://doi.org/10.1029/2024GL109621

Cochran, J. K. (1979). *The Geochemistry of 226Ra and 228Ra in Marine Deposits*. Ph.D. Thesis, Yale University, New Haven, CT.

Cook, P. G., Rodellas, V., & Stieglitz, T. C. (2018). Quantifying surface water, porewater, and groundwater interactions using tracers: Tracer fluxes, water fluxes, and end-member concentrations. *Water Resources Research*, *54(3*), 2452–2465.
https://doi.org/10.1002/2017WR021780

Diego-Feliu, M., Rodellas, V., Alorda-Kleinglass, A., Tamborski, J., van Beek, P., Heins, L., et al. (2020). Guidelines and limits for the quantification of Ra isotopes and related radionuclides with the Radium Delayed Coincidence Counter (RaDeCC). *Journal of Geophysical Research: Oceans*, *125*(*4*). https://doi.org/10.1029/2019JC015544

Dillow, J., & Greene, E. (1999). *Ground-water discharge and nitrate loadings to the coastal bays of Maryland*. (U.S. Geologic Survey Water Resources Investigations Report 99-4167). Retrieved from https://pubs.usgs.gov/wri/wri99-4167/

Eckhardt, D. A., Flipse, W. J., & Oaksford, E. T. (1986). *Relation between land use and ground-water quality in the upper glacial aquifer in Nassau and Suffolk Counties, Long Island, New York.* (U.S. Geological Survey Water-Resources Investigations Report 86-4142).
https://doi.org/10.3133/wri864142

Environmental Integrity Project. (2020). *Poultry and manure production on Virginia's Eastern Shore*. Retrieved from https://environmentalintegrity.org/wp-content/uploads/2020/04/VA-Eastern-Shore-Poultry-Report-4.22.20.pdf

Fetter, C.W. (1976). Hydrogeology of the South Fork of Long Island, New York. *GSA Bulletin*, *87(3)*, 401–406. https://doi.org/10.1130/0016-7606(1976)87<401:HOTSFO>2.0.CO;2

Garcia-Orellana, J., Cochran, J. K., Bokuniewicz, H., Daniel, J. W. R., Rodellas, V., & Heilbrun, C. (2014). Evaluation of 224Ra as a tracer for submarine groundwater discharge in Long Island Sound (NY). *Geochimica et Cosmochimica Acta*, *141*, 314–330. https://doi.org/10.1016/j.gca.2014.05.009

Garcia-Orellana, J., Rodellas, V., Tamborski, J., Diego-Feliu, M., van Beek, P., Weinstein, Y., et al (2021). Radium isotopes as submarine groundwater discharge (SGD) tracers: Review and recommendations. *Earth-Science Reviews*, *220*, 103681 https://doi.org/10.1016/j.earscirev.2021.103681

Garcia-Solsona, E., Garcia-Orellana, J., Masqué, P., & Dulaiova, H. (2008). Uncertainties associated with 223Ra and 224Ra measurements in water via a Delayed Coincidence Counter (RaDeCC). *Marine Chemistry*, *109*(*3–4*), 198–219. https://doi.org/10.1016/j.marchem.2007.11.006

Giordano, J. C. P., Brush, M. J., & Anderson, I. C. (2011). Quantifying annual nitrogen loads to Virginia's coastal lagoons: Sources and water quality response. *Estuaries and Coasts*, *34*(*2*), 297–309. https://doi.org/10.1007/s12237-010-9345-7

Gobler, C. J., Burson, A., Koch, F., Tang, Y., & Mulholland, M. R. (2012). The role of nitrogenous nutrients in the occurrence of harmful algal blooms caused by Cochlodinium polykrikoides in New York estuaries (USA). *Harmful Algae*, *17*, 64–74. https://doi.org/10.1016/j.hal.2012.03.001

Gómez, F., Richlen, M. L., & Anderson, D. M. (2017). Molecular characterization and morphology of Cochlodinium strangulatum, the type species of Cochlodinium, and Margalefidinium gen. nov. for C. polykrikoides and allied species (Gymnodiniales, Dinophyceae). *Harmful Algae*, *63*, 32–44. https://doi.org/10.1016/j.hal.2017.01.008

Gonneea, M. E., Mulligan, A. E., & Charette, M. A. (2013). Seasonal cycles in radium and barium within a subterranean estuary: Implications for groundwater derived chemical fluxes to surface waters. *Geochimica et Cosmochimica Acta*, *119*, 164–177. https://doi.org/10.1016/j.gca.2013.05.034

Hardy, C. D. (1976). *A preliminary description of the Peconic Bay estuary* (Special Report No. 74, pp. 1-65). Stony Brook, New York: Marine Sciences Research Center, Stony Brook University, Retrieved from https://commons.library.stonybrook.edu/special-reports/74

Hartl, K. M. (2006). *Facies distribution and hydraulic conductivity of lagoonal sediments in a Holocene transgressive barrier island sequence, Indian River Lagoon, Florida*. (M.S. Thesis). Retrieved from University of Florida Library (https://ufl-flvc.primo.exlibrisgroup.com/permalink/01FALSC_UFL/6ad6fc/alma990208288470306597). Gainesville, Fl: University of Florida.

Herman, J., Shen, J., & Huang, J. (2007). *Tidal flushing characteristics in Virginia's tidal embayments*. Gloucester Point, VA: Virginia Institute of Marine Science. https://doi.org/10.21220/m2-bp67-w829

Jahn, K.L., & Walter, D.A. (2025). *MODFLOW 6 and MODPATH 7 models for simulating groundwater flow and nitrogen transport in the Long Island, New York aquifer system*. [Data set]. U.S. Geological Survey data release. https://doi.org/10.5066/P14KKUF7

Kelly, N. E., Guijarro-Sabaniel, J., & Zimmerman, R. (2021). Anthropogenic nitrogen loading and risk of eutrophication in the coastal zone of Atlantic Canada. *Estuarine, Coastal and Shelf Science*, *263*, 107630. https://doi.org/10.1016/j.ecss.2021.107630

963

964 Lachat Instruments. (2020). *QuikChem® Methods List for Automated Ion Analyzers* (LL022).
965 Hach Company. Retrieved from: https://my.hach.com/flow-injection-analysis-fia/lachat-
966 quikchem-flow-injection-analysis-system/family-downloads?productCategoryId=59429623939

967

968 Lecher, A. L., Mackey, K., Kudela, R., Ryan, J., Fisher, A., Murray, J., & Paytan, A. (2015).
969 Nutrient loading through submarine groundwater discharge and phytoplankton growth in
970 Monterey bay, CA. *Environmental Science and Technology*, *49*(11), 6665–6673.
971 https://doi.org/10.1021/acs.est.5b00909

972

973 Lecher, A. L., Murray, J., & Paytan, A. (2018). Quantifying processes governing nutrient
974 concentrations in a coastal aquifer via principal component analysis. *Hydrology*, *5*(1).
975 https://doi.org/10.3390/hydrology5010015

976

977 Liu, Y., Mao, R., Yu, S., & Jiao, J. J. (2025). Seasonality of Radium Isotopes in an Intertidal
978 Aquifer. *Journal of Geophysical Research: Oceans*, *130*(*4*), e2024JC022059.
979 https://doi.org/10.1029/2024JC022059

980

981 Lloyd, S. (2014). *Nitrogen load modeling to forty-three subwatersheds of the Peconic Estuary*,
982 The Nature Conservancy & Peconic Estuary Program. Retrieved from:
983 https://www.peconicestuary.org/wp-content/uploads/2017/06/Nitrogenloadmodelingtoforty-
984 thr.pdf

985

986 Luek, J. L., & Beck, A. J. (2014). Radium budget of the York River estuary (VA, USA)
987 dominated by submarine groundwater discharge with a seasonally variable groundwater end-
988 member. *Marine Chemistry*, *165*, 55–65. https://doi.org/10.1016/j.marchem.2014.08.001

989

990 McClymonds, N. E., & Franke, O. L. (1972). *Water-transmitting properties of aquifers on Long*
991 *Island, New York* (U.S. Geological Survey Professional Paper 627-E). Washington D.C.: U.S.
992 Geological Survey. https://doi.org/10.3133/pp627E

993

McFarland, E.R., & Beach, T.A. (2019). *Hydrogeologic framework of the Virginia Eastern Shore* (Scientific Investigations Report 2019–5093, pp. 1-26). Reston, Virginia: U.S. Geological Survey. https://doi.org/10.3133/sir20195093

McGlathery, K. J., Anderson, I. C., & Tyler, A. C. (2001). Magnitude and variability of benthic and pelagic metabolism in a temperate coastal lagoon. *Marine Ecology Progress Series, 216*, 1–15. https://doi.org/10.3354/meps216001

Michael, H. A., Mulligan, A. E., & Harvey, C. F. (2005). Seasonal oscillations in water exchange between aquifers and the coastal ocean. *Nature*, *436*(*7054*), 1145–1148. https://doi.org/10.1038/nature03935

Monti, J., Jr., Walter, D. A., & Jahn, K. L. (2024). *Nitrogen load estimates from six nonpoint sources on Long Island, New York, from 1900 to 2019*. (U.S. Geological Survey Scientific Investigations Report 2024–5047). Reston, Virginia: U.S. Geological Survey. https://doi.org/10.3133/sir20245047

Moore, W. S., & Arnold, R. (1996). Measurement of 223Ra and 224Ra in coastal waters using a delayed coincidence counter. *Journal of Geophysical Research: Oceans*, *101*(*C1*), 1321–1329. https://doi.org/10.1029/95JC03139

Moore, W. S. (1999) The subterranean estuary: a reaction zone of ground water and sea water. *Marine Chemistry*, *65(1-2),* 111–125. http://dx.doi.org/10.1016/S0304-4203(99)00014-6

Moore, W. S. (2008). Fifteen years experience in measuring 224Ra and 223Ra by delayed-coincidence counting. *Marine Chemistry*, *109*(3–4), 188–197. https://doi.org/10.1016/j.marchem.2007.06.015

Moore, W. S. (2010). The effect of submarine groundwater discharge on the ocean. *Annual Review of Marine Science*, *2*, 59–88. https://doi.org/10.1146/annurev-marine-120308-081019

Moore, W. S., & Cai, P. (2013). Calibration of RaDeCC systems for 223Ra measurements. *Marine Chemistry*, *156*, 130–137. https://doi.org/10.1016/j.marchem.2013.03.002

Moore, W. S., & Joye, S. B. (2021). Saltwater intrusion and submarine groundwater discharge: acceleration of biogeochemical reactions in changing coastal aquifers. *Frontiers in Earth Science,* 9, 1-14. https://doi.org/10.3389/feart.2021.600710

Mulholland, M. R., Morse, R. E., Boneillo, G. E., Bernhardt, P. W., Filippino, K. C., Procise, L. A., et al. (2009). Understanding causes and impacts of the dinoflagellate, Cochlodinium polykrikoides, blooms in the Chesapeake Bay. *Estuaries and Coasts*, *32*(*4*), 734–747. https://doi.org/10.1007/s12237-009-9169-5

National Oceanic and Atmospheric Administration National Geophysical Data Center. (2007). *Montauk, New York 1/3 arc-second MHW coastal digital elevation model* [Data set]. NOAA National Centers for Environmental Information. Retrieved from https://catalog.data.gov/dataset/montauk-new-york-1-3-arc-second-mhw-coastal-digital-elevation-model1

Oehler, T., Tamborski, J., Rahman, S., Moosdorf, N., Ahrens, J., Mori, C., et al. (2019). DSi as a Tracer for Submarine Groundwater Discharge. *Frontiers in Marine Science*, *6*. https://doi.org/10.3389/fmars.2019.00563

Oertel, G., Kearney, M., Leatherman, S., & Woo, H. (1989). Anatomy of a barrier platform: outer barrier lagoon, Southern Delmarva Peninsula, Virginia. *Marine Geology*. *88*(*3-4*), 303-318. https://doi.org/10.1016/0025-3227(89)90103-5

Paerl, H. W., Rudek, J., & Mallin, M. A. (1990). Stimulation of phytoplankton production in coastal waters by natural rainfall inputs: Nutritional and trophic implications. *Marine Biology, 107*(2), 247–254. https://doi.org/10.1007/BF01319823

Peconic Estuary Partnership. (2007). *Total maximum daily load for nitrogen in the Peconic Estuary Program study area, including waterbodies currently impaired due to low dissolved oxygen: the lower Peconic River and tidal tributaries; Western Flanders Bay and lower Sawmill Creek; and Meetinghouse Creek, Terrys Creek and tributaries.* Yaphank, NY: Peconic Estuary Partnership. Retrieved from https://www.peconicestuary.org/total-maximum-daily-load-for-nitrogen-in-the-peconic-estuary/

Peconic Estuary Program. (2020). *Chapter 3: Nutrients Management Plan.* In *Comprehensive Conservation and Management Plan (CCMP)* (pp. 25–40). Peconic Estuary Program. Retrieved from https://www.peconicestuary.org/accordions/ccmp-docs/

Rama, & Moore, W. S. (1996). Using the radium quartet for evaluating groundwater input and water exchange in salt marshes. *Geochimica et Cosmochimica Acta, 60(23)*, 4645–4652. https://doi.org/10.1016/S0016-7037(96)00289-X

Reay, W. G., Gallagher, D. L., & Simmons, G. M., Jr. (1992). Groundwater discharge and its impact on surface water quality in a Chesapeake Bay inlet. *Water Resources Bulletin, 28*(*6*), 1121–1134. https://doi.org/10.1111/j.1752-1688.1992.tb04023.x

Richardson, D. L. (1994). *Hydrogeology and analysis of the ground-water-flow system of the Eastern Shore, Virginia* (U.S. Geological Survey Water Supply Paper 2401). Reston, Virginia: U.S. Geological Survey. https://doi.org/10.3133/wsp2401

Richardson, D. L., Porter, J. H., Oertel, G. F., Zimmerman, R. C., Carlson, C. R., Overman, K. M., & Carlson, C. L. (2024). *Integrated topography and bathymetry for the Eastern Shore of Virginia (version 12)* [Data set]. Environmental Data Initiative. https://doi.org/10.6073/pasta/2c780710fc3e74344668b0b4d3c381ea

Rocha, C., Wilson, J., Scholten, J., & Schubert, M. (2015). Retention and fate of groundwater-borne nitrogen in a coastal bay (Kinvara Bay, Western Ireland) during summer. *Biogeochemistry*, *125*(2), 275–299. https://doi.org/10.1007/s10533-015-0116-1

Rodellas, V., Garcia-Orellana, J., Trezzi, G., Masqué, P., Stieglitz, T. C., Bokuniewicz, H., et al. (2017). Using the radium quartet to quantify submarine groundwater discharge and porewater exchange. *Geochimica et Cosmochimica Acta*, *196*, 58–73. https://doi.org/10.1016/j.gca.2016.09.016

Rodellas, V., Stieglitz, T. C., Andrisoa, A., Cook, P. G., Raimbault, P., Tamborski, J. J., et al. (2018). Groundwater-driven nutrient inputs to coastal lagoons: The relevance of lagoon water recirculation as a conveyor of dissolved nutrients. *Science of the Total Environment*, *642*, 764–780. https://doi.org/10.1016/j.scitotenv.2018.06.095

Ruiz-González, C., Rodellas, V., & Garcia-Orellana, J. (2021). The microbial dimension of submarine groundwater discharge: Current challenges and future directions. *FEMS Microbiology Reviews 45*(*5*). https://doi.org/10.1093/femsre/fuab010

Santos, I. R., Burnett, W. C., Chanton, J., Mwashote, B., Suryaputra, I. G. N. A., & Dittmar, T. (2008). Nutrient biogeochemistry in a Gulf of Mexico subterranean estuary and groundwater-derived fluxes to the coastal ocean. *Limnology and Oceanography*, *53*(*2*), 705–718. https://doi.org/10.4319/lo.2008.53.2.0705

Santos, I. R., Burnett, W. C., Dittmar, T., Suryaputra, I. G. N. A., & Chanton, J. (2009). Tidal pumping drives nutrient and dissolved organic matter dynamics in a Gulf of Mexico subterranean estuary. *Geochimica et Cosmochimica Acta*, *73*(*5*), 1325–1339. https://doi.org/10.1016/j.gca.2008.11.029

Santos, I. R., Peterson, R. N., Eyre, B. D., & Burnett, W. C. (2010). Significant lateral inputs of fresh groundwater into a stratified tropical estuary: Evidence from radon and radium isotopes. *Marine Chemistry, 121(1-4),* 37–48. https://doi.org/10.1016/j.marchem.2010.03.003

Santos, I. R., Eyre, B. D., & Huettel, M. (2012). The driving forces of porewater and groundwater flow in permeable coastal sediments: A review. In *Estuarine, Coastal and Shelf Science*, *98*, 1–15. https://doi.org/10.1016/j.ecss.2011.10.024

Santos, I. R., Chen, X., Lecher, A. L., Sawyer, A. H., Moosdorf, N., Rodellas, V., et al. (2021). Submarine groundwater discharge impacts on coastal nutrient biogeochemistry. *Nature Reviews Earth and Environment*, *2(5),* 307-323. https://doi.org/10.1038/s43017-021-00152-0

Scavia, D., & Bricker, S. B. (2006). Coastal eutrophication assessment in the United States. *Biogeochemistry, 79*(*2*), 187–208. https://doi.org/10.1007/s10533-006-9011-0

Schubert, C. E. (1998). *Areas contributing ground water to the Peconic Estuary, and ground-water budgets for the North and South Forks and Shelter Island, eastern Suffolk County, New York* (U.S. Geological Survey Water-Resources Investigations Report 97-4136). Coram, New York: U.S. Geological Survey. https://doi.org/10.3133/wri974136

Schubert, M., Paschke, A., Lieberman, E., & Burnett, W. C. (2012). Air–water partitioning of 222Rn and its dependence on water temperature and salinity. *Environmental Science & Technology, 46*(*7),* 3905–3911. https://doi.org/10.1021/es204680n

Slomp, C. P., & Van Cappellen, P. (2004). Nutrient inputs to the coastal ocean through submarine groundwater discharge: Controls and potential impact. *Journal of Hydrology*, *295*(*1–4*), 64–86. https://doi.org/10.1016/j.jhydrol.2004.02.018

Smith, C. G., & Swarzenski, P. W. (2012). An investigation of submarine groundwater-borne nutrient fluxes to the west Florida shelf and recurrent harmful algal blooms. *Limnology and Oceanography*, *57*(2), 471–485. https://doi.org/10.4319/lo.2012.57.2.0471

Stanhope, J. W., Anderson, I. C., & Reay, W. G. (2009). Base flow nutrient discharges from lower Delmarva Peninsula watersheds of Virginia, USA. *Journal of Environmental Quality*, *38*(*5*), 2070–2083. https://doi.org/10.2134/jeq2008.0358

Stringer, C. E., & Burnett, W. C. (2004). Sample bottle design improvements for radon emanation analysis of natural waters. *Health physics*, *87*(6), 642-646.

Stumm, F., Finkelstein, J. S., Williams, J. H., & Lange, A. D. (2024). *Hydrogeologic framework and extent of saltwater intrusion in Kings, Queens, and Nassau Counties, Long Island, New York* (U.S. Geological Survey Scientific Investigations Report 2024–5048, 83 p.). U.S. Geological Survey. https://doi.org/10.3133/sir20245048

Swarzenski, P. W. (2007). U/Th series radionuclides as coastal groundwater tracers. *Chemical Reviews*, *107*(*2*), 663–674. https://doi.org/10.1021/cr0503761

Tamborski, J. J., Cochran, J. K., & Bokuniewicz, H. J. (2017a). Application of 224Ra and 222Rn for evaluating seawater residence times in a tidal subterranean estuary. *Marine Chemistry*, *189*, 32–45. https://doi.org/10.1016/j.marchem.2016.12.006

Tamborski, J. J., Cochran, J. K., & Bokuniewicz, H. J. (2017b). Submarine groundwater discharge driven nitrogen fluxes to Long Island Sound, NY: Terrestrial vs. marine sources. *Geochimica et Cosmochimica Acta*, *218*, 40–57. https://doi.org/10.1016/j.gca.2017.09.003

Tamborski, J. J., Cochran, J. K., Bokuniewicz, H., Heilbrun, C., Garcia-Orellana, J., Rodellas, V., & Wilson, R. (2020). Radium mass balance sensitivity analysis for submarine groundwater discharge estimation in semi-enclosed basins: The case study of Long Island Sound. *Frontiers in Environmental Science*, *8,* 108. https://doi.org/10.3389/fenvs.2020.00108

Taniguchi, M., Dulai, H., Burnett, K. M., Santos, I. R., Sugimoto, R., Stieglitz, T., et al. (2019). Submarine groundwater discharge: Updates on its measurement techniques, geophysical drivers, magnitudes, and effects. *Frontiers in Environmental Science, 7*, 141. https://doi.org/10.3389/fenvs.2019.00141

Turekian, K. K., Tanaka, N., Turekian, V. C., Torgersen, T., & Deangelot, E. C. (1996). Transfer rates of dissolved tracers through estuaries based on 228Ra: a study of Long Island Sound. *Continental Shelf Research, 16(7),* 863-873. http://dx.doi.org/10.1016/0278-4343(95)00039-9

Tyler, A. C. (2002). *Impact of benthic algae on dissolved organic nitrogen in a temperate, coastal lagoon* (Doctoral dissertation). Retrieved from Virginia Coast Reserve Long-Term Ecological Research Student Theses and Dissertations. (https://www.vcrlter.virginia.edu/thesis/). Charlottesville, Virginia: University of Virginia.

USEPA. (1993). *Method 300.0: Methods for the determination of inorganic substances in environmental samples* (EPA-600/4-93-100). U.S. Environmental Protection Agency, Environmental Monitoring Systems Laboratory. Retrieved from: https://monitoringprotocols.pbworks.com/f/EPA600-R-63-100.pdf

USEPA. (1997). *Method 366.0: Determination of dissolved silicate in estuarine and coastal waters by gas segmented continuous flow colorimetric analysis,* EPA/600/R-97/072. U.S. Environmental Protection Agency, Environmental Monitoring Systems Laboratory. Retrieved from: https://www.nemi.gov/methods/method_summary/4661/

Valiela, I., Collins, G., Kremer, J., Lajtha, K., Geist, M., Seely, M., Brawley, J., & Sham, C. H. (1997). Nitrogen loading from coastal watersheds to receiving estuaries: New method and application. *Ecological Applications*, *7(2),* 358-380. https://doi.org/10.1890/1051-0761(1997)007[0358:NLFCWT]2.0.CO;2

Virginia Department of Environmental Quality. (2021). *Environmental Data Mapper (EDM)* [Dataset]. Virginia Environmental Data Hub. https://apps.deq.virginia.gov/EDM/

Walter, D. A., Masterson, J. P., Finkelstein, J. S., Monti, J., Jr., Misut, P. E., & Fienen, M. N. (2020). *Simulation of groundwater flow in the regional aquifer system on Long Island, New York, for pumping and recharge conditions in 2005–15*. (U.S. Geological Survey Scientific Investigations Report 2020–5091, 75 p). https://doi.org/10.3133/sir20205091

Waska, H., Kim, S., Kim, G., Peterson, R. N., & Burnett, W. C. (2008). An efficient and simple method for measuring 226Ra using the scintillation cell in a delayed coincidence counting

system (RaDeCC). *Journal of Environmental Radioactivity*, *99*(*12*), 1859–1862. https://doi.org/10.1016/j.jenvrad.2008.08.008

Wilson, S. J., Anderson, I. C., Song, B., & Tobias, C. R. (2023). Temporal and spatial variations in subterranean estuary geochemical gradients and nutrient cycling rates: Impacts on groundwater nutrient export to estuaries. *Journal of Geophysical Research: Biogeosciences*, *128(6),* e2022JG007132 . https://doi.org/10.1029/2022JG007132

Wilson, S. J., Song, B., Anderson, I. C., & Tobias, C. R. (2024a). Nitrification in a subterranean estuary: An ex situ and in situ method comparison determines nitrate is available for discharge. *Journal of Geophysical Research: Biogeosciences*, *129*(*6*), e2023JG007876 https://doi.org/10.1029/2023JG007876

Wilson, S. J., Moody, A., McKenzie, T., Cardenas, M. B., Luijendijk, E., Sawyer, A. H., et al. (2024b). Global subterranean estuaries modify groundwater nutrient loading to the ocean. *Limnology And Oceanography Letters*, *9(4),* 411–422. https://doi.org/10.1002/lol2.10390

Wilson, S. J., Tamborski, J. J., Song, B., Bernhardt, P., & Mulholland, M. R. (2024c). Submarine groundwater discharge as a major nutrient source in river-fed vs. tidally dominated estuaries. *Limnology and Oceanography*, *70(2),* 426-442. https://doi.org/10.1002/lno.12772

Xu, H., Xu, B., Yu, H., Zhao, S., Burnett, W. C., Yao, Q., et al. (2024). Deciphering multi-scale submarine groundwater discharge in a typical eutrophic bay. *Journal of Geophysical Research: Oceans*, *129(6),* e2024JC021042. https://doi.org/10.1029/2024JC021042

Xun, Z. & Ying, W. (2009). Brief review on methods of estimation of the location of a fresh water–salt water interface with hydraulic heads or pressures in coastal zones. *Groundwater Monitoring & Remediation*, *29(4)*, 77-84. https://doi.org/10.1111/j.1745-6592.2009.01259.x

1234 Zhu, D., Liu, S. M., Leynaert, A., Tréguer, P., Ren, J., Schoelynck, J., et al. (2024). Muddy
1235 sediments are an important potential source of silicon in coastal and continental margin zones.
1236 *Marine Chemistry*, *258*, 104350. https://doi.org/10.1016/j.marchem.2024.104350